AN ABSTRACT OF THE THESIS OF

Von Trullinger for the degree of Master of Science in Electrical and Computer Engineering presented on July 22, 2004.

Title: Physical Layer Design of a Robust Low-Power Low-Complexity Optical Wireless Sensor System with Angular Diversity for Metal-Enclosed Environments.

Abstract approved: _____

Huaping Liu

The desire to apply short-range wireless communication systems to telemetry sensor networks in a metal-enclosed chamber has prompted this study. This thesis will discuss the design of an infrared (IR) communication system for a wireless low-power, low-data-rate sensor network in a metal enclosure. This design requires an in-depth understanding of the environment and how IR will propagate in it. The metal enclosure offers the advantage of little background (ambient) lighting noise, which is the main noise source in IR communication. Also, due to the small dimensions of this enclosure, the non-line-of-sight (NLOS) communication will take advantage of the reflected paths off the walls. To improve system performance in this diffuse NLOS communication environment, angular diversity will be employed and tested. It will be shown that these diffuse reflections are an advantage at low data rates ($< 1Mbps$), but then become a hindrance at higher data rates ($> 10Mbps$) due to inter-symbol interference (ISI) caused by channel excess delay. All measurement results, including bit error rate (BER) versus transmitted power, will be presented.

©Copyright by Von Trullinger

July 22, 2004

All Rights Reserved

Physical Layer Design of a Robust Low-Power Low-Complexity Optical Wireless Sensor System with Angular Diversity for Metal-Enclosed Environments

by

Von Trullinger

A THESIS

submitted to

Oregon State University

in partial fulfillment of
the requirements for the
degree of

Master of Science

Presented July 22, 2004
Commencement June 2005

Master of Science thesis of Von Trullinger presented on July 22, 2004.

APPROVED:

Major Professor, representing Electrical and Computer Engineering

---

Director of the School of Electrical Engineering and Computer Science

---

Dean of Graduate School

I understand that my thesis will become part of the permanent collection of Oregon State University libraries. My signature below authorizes release of my thesis to any reader upon request.

Von Trullinger, Author

ACKNOWLEDGMENTS

I would first like to acknowledge the people who made this project possible: My advisor, Prof. Huaping Liu from Oregon State University, for his inspiration and guidance through this thesis, for providing me the opportunity to work on some exciting research over the past two years, and for providing a research assistantship which sustained me financially; Dr. Ratish Punnoose (Sandia Liaison) for providing mentorship while I interned at Sandia and for many of the new ideas presented in this thesis; and Prof. Tom Plant for his guidance in and out of the classroom.

Funding for this project was provided by Sandia National Laboratories and the Center for Design of Analog and Digital Integrated Circuits (CDADIC).

I am deeply indebted to my supervisor Prof. Huaping Liu , whose help, stimulating suggestions and encouragement assisted me throughout the research and writing of this thesis.

Thank you to all the thesis committee members - Dr. Huaping Liu, Dr.Tom Plant, Dr. Jimmy Yang and Dr. Ratish Punnoose, for taking the time to serve on my defense committee. I thank Ferne Simendinger and all the staff members of the Electrical Engineering department, who had the answers for all my administrative questions and needs.

I would also like to thank my friends and colleagues Sudheer, Vinod, Rahul, Tai, Joshua, Jie, Yu, David, Robert, and Can for the invigorating discussions which have enriched me in various topics. I have made a lot of friends here, who have been a source of constant encouragement and support. I wish to thank all of these friends and groups, including Ben, Kurt, Lee, Clint, our WCC Community Group, High School Youth Group and Willamette Community Church.

Above all, I thank my family for supporting me in all my endeavors. I would like to thank my wife, Elisa, for her daily love and support, late night dinners, and encouraging notes. Last but not least, I thank God for all that he has blessed me with.

TABLE OF CONTENTS

Page

1. INTRODUCTION 1

1.1. Thesis Organization 2

1.2. Previous Work 2

1.3. Communication Channel 3

1.3.1. Frequency Response and Impulse Response of RF Channels 3
1.3.2. Frequency Response and Impulse Response of Optical Channels 4
Analytical Calculation of Delay Spread for Optical Channels 5
Shadowing and Receiver Tilt 6
Atmospheric Loss 6
ISI 7
Infrared Behavior 7
Sources of Optical Noise 7
Noise Breakdown 8

2. IR COMMUNICATION BACKGROUND 10

2.1. Baseband Modulation Schemes 10

2.1.1. OOK 10
2.1.2. PPM 12
PPM Synchronization 14
PPM Slot Synchronization 15
Frame Synchronization 16
2.1.3. DPPM 17

2.2. Optical Components 18

2.2.1. Optical Sources 18
Light Emitting Diode 19
Laser Diode 19
2.2.2. Optical Detectors 19
Photodiodes 19
Avalanche Photodiodes 19

2.3. Device Physics 20

2.3.1. Light Emitting Diode 21
2.3.2. Light Absorbing Diode 22

TABLE OF CONTENTS (Continued)

Page

2.4. Comparison of RF and Optical Communication Systems 26
2.4.1. Link Analysis Comparison Between IR and RF 27

3. SYSTEM ARCHITECTURE 30

3.1. Prototype 30
3.1.1. System Requirements 30
3.1.2. System Specification 31

3.2. Transmitter 31
3.2.1. Analog Front-End 31
3.2.2. Baseband Transmitter 32

3.3. Receiver 35
3.3.1. Analog Front-End 36
Infrared Portion 39
3.3.2. Baseband Receiver 41
Channel 42

3.4. Diversity 42

4. RESULTS 45

4.1. Theoretical Analysis 45
4.1.1. Link Budget Analysis 46
Receiver Sensitivity Budget 47

4.2. Simulation Results 49
4.2.1. Digital Simulation in MATLAB 49
4.2.2. Analog Simulation of Frontend in Spice 50

4.3. Experimental Results 53
4.3.1. RF Channel Measurements 53
4.3.2. Optical Response of Different Materials 56
4.3.3. Bit Error Rate Performance 60
Power vs. BER 60
Data Rate vs. BER 61
Distance vs. BER 61

TABLE OF CONTENTS (Continued)

Page

Angular Diversity 62
Return-to-Zero Line Coding Performance 62
4.3.4. General Experimental Comments and Observations 63
Background Light 63
Measured Optical Power from Transmitter 64

5. CONCLUSION 67

5.1. Summary of Results 67

5.2. Summary of Contributions 68

5.3. Future Research 69

5.3.1. Advanced Topics 69
Positioning 70
Diversity Techniques 70
Power Efficient Modulation 70
Clock Recovery 70
Front End Amplifier 70
5.3.2. Digital Processing Algorithms for IR 71
Spreading 71
Coding 71
Pulse Shaping 72
Equalization 72

APPENDICES 73

A Appendices 73

A1. Abbreviations 74
A2. Prototype Bill of Material (BOM) 77
A3. Prototype Pictures 77
A4. FPGA AHDL Source Code 80
100kbps NRZ-OOK 80
100kbps NRZ-OOK 85

BIBLIOGRAPHY 91

LIST OF FIGURES

Figure		Page
2.1	OOK and PPM Line Coding Formats (Courtesy of [2])	11
2.2	A PPM signal with L = 4 and x = $\frac{1}{2}$ [17]	13
2.3	Block Diagram of a Maximum Likelihood PPM Demodulator [17]	13
2.4	Block Diagram of an Efficient PPM Demodulator [17]	14
2.5	Basic Synchronization Architecture For a PPM Receiver [17]	15
2.6	PN-Diode Cross-Section [19]	23
2.7	Bias Voltage vs. Capacitance For Different Photodiode areas [19]	24
2.8	Diode Responsivity vs. Wavelength For Two Bias Conditions [19]	25
3.1	Block Diagram of the Infrared Communication System	31
3.2	Spectrum of 880 nm LED [25]	32
3.3	Optical Power vs. Electric Current for OD-880E (Courtesy of Opto Diode)	34
3.4	Optical Front-End Schematic of the Transmitter	34
3.5	PN9 Schematics	35
3.6	50%-duty-cycle return-to-zero data encoder	35
3.7	Direct Detection Receiver	37
3.8	Optical Front-End Schematic of the Receiver	39
3.9	Optical Front-End Schematic of the Transmitter with Diversity	43
3.10	Receiver Selection Diversity Schematic	43
4.1	Generalized Optical Communication Link [20]	45
4.2	Components of a Communication System Link Budget ([20]	47
4.3	Link Budget for 0.1Mbps Optical Sensor	48
4.4	Receiver Sensitivity Budget	49

LIST OF FIGURES (Continued)

Figure Page

4.5 Simulation with Theoretical Validation for OOK & 4-PPM in an AWGN Channel 51

4.6 Photodiode Circuit Model [24] 52

4.7 Photodiode Circuit Temporal Response 52

4.8 Photodiode Circuit Frequency Response 53

4.9 Test RF Enclosure 54

4.10 Frequency Response for the LOS Closed Box 56

4.11 Frequency Response for the LOS Open Box 56

4.12 Frequency Response for the NLOS Closed Box 57

4.13 Frequency Response for the NLOS Open Box 57

4.14 Impulse Response for the LOS Closed Box 58

4.15 Impulse Response for the LOS Open Box 58

4.16 Impulse Response for the NLOS Closed Box 59

4.17 Impulse Response for the NLOS Open Box 59

4.18 Optical Power in Milliwatts Versus Bit Error Rate 61

4.19 Transmitter Current in Milliamps Versus Bit Error Rate ($A_{PD} = 100mm^2$) 62

4.20 Datarate in Kbps Versus Bit Error Rate ($A_{PD} = 100mm^2$) 63

4.21 Datarate in Kbps Versus Bit Error Rrate at Two Different Temperatures 64

4.22 Distance Versus Bit Error Rate ($A_{PD} = 100mm^2$) 65

4.23 Transmitter Current Versus BER for Different Diversity Schemes ($A_{PD} = 35mm^2$) 65

4.24 Return-to-Zero Encoder 66

4.25 Transmitter Current versus BER for Different Line-Coding Schemes ($A_{PD} = 35mm^2$) 66

5.1 Inside of Metal Enclosure 77

LIST OF FIGURES (Continued)

Figure Page

5.2 Outside of Metal Enclosure 78

5.3 Transmitter Front-End 78

5.4 Receiver Front-End with $35mm^2$ PD 79

5.5 Receiver Front-End with $100mm^2$ PD 79

LIST OF TABLES

Table		Page
2.1	4-DPPM Mapping	18
2.2	Radiant Wavelengths of Different Semi-Conductor Materials	22
2.3	Properties of Optical and Radio Channels. [13]	28
2.4	IR versus RF link budget	29
3.1	System Specifications	30
3.2	OP-880E LED Specifications	33
3.3	Photo Diode Specifications	44
4.1	Theoretical Performance Equations of OOK and PPM Modulation [2]	50
4.2	RMS Delay Spread for different LOS and NLOS situations	55
4.3	Optical Response of Different Materials ($100mm^2$ PD)	60
5.1	Bandwidth Limitations For the System Designed	69

PHYSICAL LAYER DESIGN OF A ROBUST LOW-POWER LOW-COMPLEXITY OPTICAL WIRELESS SENSOR SYSTEM WITH ANGULAR DIVERSITY FOR METAL-ENCLOSED ENVIRONMENTS

CHAPTER 1. INTRODUCTION

This thesis gives an account of an investigation into the use of infrared communication in a metal-enclosed environment for aerospace applications. The wireless systems objective is to reduce cable mass and increase thermal isolation in commercial, military, and space applications. Specific target applications include commercial aircraft landing gear and other sensors where wiring represents a difficult protection problem with high weight and cost. The channel characterization study for the military application targets the hub-sensor communication within the re-entry vehicle. This new focus also targets spacecraft sensors to decrease launch costs associated with cable mass. The next generation space telescope is also a target application to eliminate the thermal barrier penetration represented by wiring between the telescope and the signal processing and control electronics.

These applications bring up a variety of questions: What range can an optical system exhibit given a limited power requirement? Which modulation schemes are the best for diffuse NLOS optical systems? What interferers exist and how can they be combated? What effect does ambient temperature have on the system? What digital baseband processing algorithms are most effective? Which optical components are well suited for this application? and How does optical communication compare to the conven-

tional radio-frequency communication? This thesis attempts to answer these questions by reviewing other research that has been conducted and building a prototype infrared system in a mock metal enclosure.

In recent years, wireless optical communication has been an area of profound research. A summary of some of that work will be presented in Section 1.2.

1.1. Thesis Organization

Chapter 1 discusses the channel environment and motivation for such a system. The background of infrared communication is presented in Chapter 2 along with the differences between wireless radio frequency (RF) and infrared (IR). Chapter 3 discusses the infrared communication system architecture, prototype, and how testing was performed. The analytical, theoretical, and measured results are presented in Chapter 4. Concluding remarks, significant contributions, advanced topics, and future work are provided in Chapter 5.

1.2. Previous Work

Existing research on IR communication systems has focused on the NLOS indoor office environment and the LOS outdoor environment [1] [2]. Infrared wireless communication is being used in such devices as home electronic remote controls, electronic keys, general input and control, game controllers, computer mice, microphones and many other applications. Other areas that have been researched for optical communication are the optical channel [3] [4] [5], effects of different modulation schemes [6], application of diversity (specifically angle diversity) [7], equalization [8], spread spectrum techniques [9], and pulse shaping in the transmitter [10]. Very little research has been conducted in the area of wireless diffuse optical communication within a small metal enclosure.

The only standards effecting this medium are Infrared Data Association(IRDA)

[11] and an optional infrared physical layer for 802.11 [12]. The IRDA standard has data rates ranging from 14.4Kbps to 16Mbps using on-off keying (OOK) and pulse position modulation (PPM) schemes with a maximum link distance of one meter. The only influential regulation that affects optical communication is a modification made to the IEC-825-1 Eye Safety Regulation which limits the maximum transmit irradiance. This affects both light emitting diode (LED) and laser diode (LD) based systems. Other than this IEC regulation, optical communication is virtually un-regulated.

1.3. Communication Channel

The mock channel environment consists of a tin metal enclosure approximately $0.5m^3$ with metal obstructions in the line-of-sight (LOS) path between the transmitter and receiver. The surface of the enclosure and obstructions will be anodized aluminum, shiny tin and white paint. For infrared, the presence of metals does not matter as much as the optical properties of the facades. The wireless infrared channel is unique, combining the filtered Gaussian-noise characteristics of a conventional wire-based channel with the Intensity Modulated Direct Detected (IM/DD) constraints of a fiber-optic system [13].

Non-directed IM/DD channels can be well characterized by their path loss and delay spread. This simplified channel characterization is due to the strong correlation between the multipath power requirement and delay spread [3]. This only applies to baseband modulation schemes, such as OOK, PPM and differential PPM (DPPM).

1.3.1. Frequency Response and Impulse Response of RF Channels

The increasing interest in this application of wireless sensors requires knowledge about reflective metal enclosures in the gigahertz to terahertz range. Key measures for describing this channel are the Frequency Response and Impulse Response. The Frequency Response can reveal the Coherence Bandwidth and the Impulse Response can

disclose the delay that a transmitted signal experiences in the multipath environment. These multipath propagation delays cause echoes or what is commonly referred to as time dispersion. The delay spread can be calculated from analytical, simulated, or measured data. In this thesis we will present analytical and measured results in Section 4.3.1.

The delay spread is depicted in the channel power delay profile, and is useful since the inter-symbol interference (ISI), which limits high bit-rate digital communication systems, is related to this parameter. ISI is related to the root mean square (RMS) delay spread of Rayleigh fading channels having wide-sense stationary uncorrelated scattering (WSSUS) characteristics [14].

The relationship between RMS delay spread and coherence bandwidth was given in [15]. The multipath intensity profile contains complete information of the temporal dispersion, which is a result of multipath scattering. The coherence bandwidth is one of the key indicators that determines whether the channel is frequency selective or not for a given information bandwidth. If the coherence bandwidth is less than the transmission bandwidth, channel protection techniques such as coding, diversity or equalization, need to be employed [14].

1.3.2. Frequency Response and Impulse Response of Optical Channels

IR channels are subject to multipath dispersion, which causes inter-symbol interference (ISI). The effects of ISI are especially severe in diffuse high data-rate systems [6]. ISI is not a concern for systems with a bit-rate below 10Mbps. Multipath fading is also not a problem because the infrared wavelength is several orders of magnitude smaller than the photodiode detector. A $100mm^2$ photodetector has about 10,000 square wavelengths contained within its dimensions. The total photocurrent produced by the photodetector is proportional to the integral of the squared electric field over the whole surface. The large surface area thus provides an inherent spatial diversity, which prevents multipath

fading. Equivalently, the photodetector can be viewed as a large two-dimensional array of miniature square-law antennas with equal gain combining [13].

Analytical Calculation of Delay Spread for Optical Channels

To analytically model the multipath dispersion, the Ceiling-Bounce Model [3] will be used to derive the channel impulse response, which is given as

$$h(t) = \frac{\rho A}{3\pi H^2} \cdot \frac{6(2H/c)^6}{(t+2H/c)^7} \cdot u(t) \tag{1.1}$$

where ρ is the plane reflectivity, A is the photodiode area, H is the distance to the dominant reflection point, c is the velocity of light, t is time, and $u(t)$ is the unit step function. Channel impulse response $h(t)$ can be written in the following simplified form:

$$h(t) = G_o \cdot \frac{6a^6}{(t+a)^7} \cdot u(t) = G_o \cdot h_c(t,a) \tag{1.2}$$

where G_o and a are given as

$$G_o = \frac{\rho A}{3\pi H^2} \tag{1.3}$$

$$a = \frac{2H}{c}. \tag{1.4}$$

The following relations give the delay spread and 3-dB cutoff frequency for the ceiling-bounce model:

$$D(h_c(t,a)) = \frac{a}{12}\sqrt{\frac{13}{11}} \tag{1.5}$$

$$f_{3dB}(h_c(t,a)) = \frac{K}{4\pi D(h_c(t,a))} \tag{1.6}$$

where K is derived in the following way:

$$K = \left| \int_0^\infty \frac{e^{j6Ku\sqrt{11/13}}}{(1+u)^7} du \right| = \frac{1}{6\sqrt{(2)}} = 0.925 \tag{1.7}$$

Another option to model the channel would be the exponential-decay model, but the ceiling-bounce model provides a slightly better fit [3].

Shadowing and Receiver Tilt

Shaddowing and the effects of receiver tilt can only be calculated and understood by experimentation or ray tracing methods.

Atmospheric Loss

The power budget and overall performance of a free space link are determined by atmospheric loss along the propagation path [16]. This loss is comprised of free space loss, scattering, refraction, shadowing and scintillation.

Free space loss defines the proportion of optical power arriving at the receiver that is captured within the receiver's aperture. Scattering and refraction due to water droplets refer to the attenuating effect of fog and mist on the power that reaches the receiver. Scintillation is the result of heating small pockets of air to slightly different temperatures, thereby creating regions of varying refractive index along the propagation path. Shadowing occurs when opaque objects shadow the receiver, thereby blocking the transmitted signal. In this application, the diffuse channel shadowing should not have a significant impact due to the many propagation paths available. Scintillation is generally not significant for distances less than 500 meters.

The line-of-sight path loss can be approximated from the following equation, which comes from the ceiling bounce model provided by [3]

$$G_{o,LOS} = \frac{\rho A}{3\pi H^2}. \tag{1.8}$$

The following equation could be used to determine the loss due to multiple reflections:

$$G_{o,NLOS} = G_{o,LOS} - n \cdot \rho_{dB} \tag{1.9}$$

where n is the number of reflections and ρ_{dB} is the average planar reflection coefficient in decibels. With a $100mm^2$ photodiode area the typical path loss with one reflection ranges from 50 dB to 75 dB over a range of one to three meters.

ISI

The link loss of an LOS system is smaller than an NLOS system, which establishes an indirect transmission link by means of reflections. These reflections limit the data bandwidth, due to multipath ISI, to less than 10Mbps unless equalization techniques are employed in the receiver or pre-processing in the transmitter. Another method to decrease ISI is to decrease the field of view (FOV) of the photodiode receiver. The best implementation of the decreased FOV is accomplished by receiver diversity, where each detector in the receiver has a smaller field of view. Together they have the same coverage as in the single detector case, but once the diversity algorithm has been executed only one detector with a smaller FOV will be enabled. Thus the multipath reflections incident on the other diversity receivers will be ignored.

Infrared Behavior

In a general sense, near infrared light can be considered just like visible light due to their spectrums being so close together. IR is absorbed by dark objects, diffusely reflected by light-colored objects, and specularly reflected from shiny surfaces. IR can penetrate glass, but not walls or other opaque materials [1]. Some opaque materials may include smoke or fog, which may be present in a metal enclosed environment.

Our diffuse link will exploit the excellent reflective properties of our aerospace enclosure surface (anodized aluminum, tin or a bright white surface). The reflected power coefficient of aluminum typically ranges from 90% to 99% with a nominal value of 95%.

Sources of Optical Noise

The noise $N(t)$ can be broken into four elements: photon noise or shot noise, gain noise, receiver circuit or thermal noise, and periodic noise. Photon noise is due to background light sources, such as sun , fluorescent, or incandescent light.

Since the background light striking the detector is normally much stronger

than the signal light, we can neglect the dependency of $N(t)$ on $X(t)$ and consider the photon noise to be additive white Gaussian noise (AWGN) with two sided power spectral density. Gain noise arises from the use of an avalanche photodiode (APD), though the overall effect is an improvement in SNR due to the lower gain required by the preamplifier. The avalanching effect of the APD has a random nature which causes gain noise. Receiver noise is due to thermal effects in the receiver circuitry, and is particularly dependent on the type of preamplifier used. Periodic noise is the result of the variation of the fluorescent lighting due to the method of driving the lamp using a ballast circuit. This generates a periodic signal with a fundamental frequency of 22KHz to 45KHz with significant harmonics to several MHz. The effect of periodic noise can be avoided by using high-pass filtering techniques.

Wireless infrared links are subject to intense ambient light that gives rise to a high-rate, signal-independent shot noise. The power spectral density of ambient induced noise extends from DC to typically a few tens of kilohertz. By applying a line code that contains no low frequency components, ambient interference can be filtered out and completely avoided [1].

In the case of this enclosure no ambient light will be present. When such ambient light is absent, the dominant noise is preamplifier thermal noise, which is Gaussian. Therefore, $N(t)$ is modeled as white, Gaussian, and is independent of signal $X(t)$.

Noise Breakdown

A silicon photodiode will be used in the receiver of the proposed prototype that will be discussed further in Chapter 3. The noise generated by a silicon photodiode, operating under reverse bias conditions, is a combination of shot noise and Johnson noise. Equation (1.10) presents an approximation for the shot noise which stems from the dark leakage current. Equation (1.11) presents a method for calculating the Johnson noise current which is caused by the shunt resistance of the device and the ambient

temperature.

$$I_S = \sqrt{2 \cdot I_d \cdot B} \tag{1.10}$$

$$I_j = \sqrt{\frac{4KTB}{R}} \tag{1.11}$$

where I_d is the leakage current, B is the system bandwidth, K is Boltzmanns constant ($1.38 \cdot 10^{-23} J/K$), T is absolute temperature, and R is shunt resistance.

The Johnson noise and shot noise will be provided by the manufacturer in the form of noise equivalent power (NEP), which is dependent on bandwidth and given in terms of $Watts/\sqrt{Hz}$. The noise equivalent power is defined as the point where the noise power level equals the signal power, i.e. SNR = 1.

CHAPTER 2. IR COMMUNICATION BACKGROUND

This chapter presents the foundational material needed to fully understand IR communication and its application to the problem being addressed.

2.1. Baseband Modulation Schemes

The emphasis in low power optical systems is to use a modulation scheme with a low duty cycle, since the narrower the pulse duration the lower the power required. Although, the narrower the optical pulse, the wider the bandwidth required by the system. Therefore, a narrower pulse will increase the power efficiency, but decrease the bandwidth efficiency.

Commonly used modulation schemes for infrared communication include non-return to zero (NRZ) OOK, return to zero (RZ) OOK, L-ary pulse position modulation (PPM), differential PPM (DPPM), quadrature amplitude modulation (QAM), quadrature phase shift keying (QPSK), AB-QAM, and pulse amplitude modulation (PAM). The simplest and most common modulation schemes are OOK, PPM, and DPPM and will be discussed in the following subsections.

2.1.1. OOK

On-off-keying (OOK) is by far the simplest and easiest to implement modulation scheme. The transmitter consists of a circuit that drives the LED directly by the baseband modulated symbols. Theoretically the receiver operates by integrating and dumping the current from the photodiode transimpedance amplifier. The integrand is then sampled and held for a comparator circuit which outputs the binary data. The

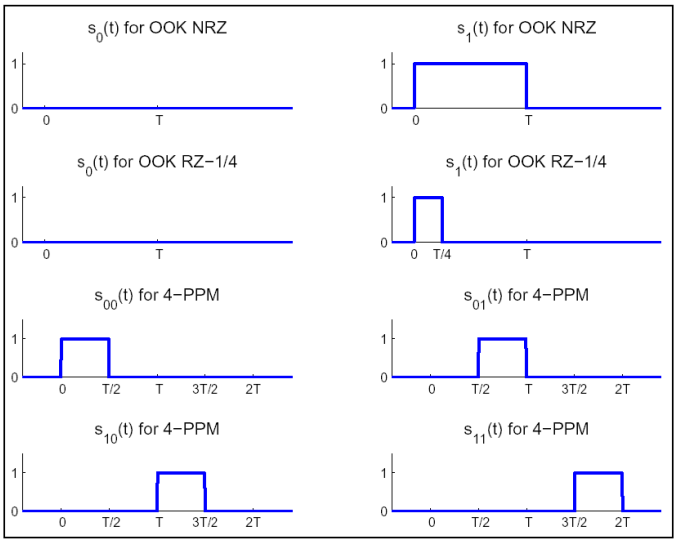

FIGURE 2.1: OOK and PPM Line Coding Formats (Courtesy of [2])

other input to the comparator is an average of the received current (i_{avg}) multiplied by the bit duration (T_{bit}). The threshold of the comparator is derived dynamically since the noise and link distance is unknown. The i_{avg} component is determined by AC-coupling the output of the front-end receiver. This averages the received signal over a certain time span that is determined by the RC time constant. If a sequence is predominated by ones or zeros the threshold drifts in either direction, thereby deteriorating the bit-error-rate (BER) performance. By increasing the averaging time, the risk of threshold drift is reduced. However, by doing this, the receiver sensitivity for slowly varying parasitic signals increases. OOK receivers are the least complex when it comes to synchronization, due largely to the relatively simple timing recovery needed for bit synchronization. Figure 2.1 defines the different RZ and NRZ OOK formats and their assigned bit values along with 4-PPM.

2.1.2. PPM

In terms of power efficiency, pulse position modulation (PPM) outperforms all other modulation schemes. Half-pulse PPM is preferred over normal PPM due to the ease of slot synchronization. Though PPM receivers are more difficult to implement because, apart from symbol/bit synchronization, frame synchronization is also required. PPM receivers are based on the maximum likelihood principle rather than threshold detection which is used in OOK. There is an integrate, dump, sample, and hold (IDSH) circuit for each time slot within a PPM frame. All the IDSH blocks are fed in parallel into a multiple input comparator (MIC) which chooses the largest signal and then outputs the associated bits. The IDSH blocks use the recovered slot timing. The comparator gets its timing from the output of the frame timing recovery circuit. A block diagram representation of the PPM scheme is given in Figure 2.2.

The following is provided as a summary of a low-power low-complexity PPM system proposed by Otte in [17].

In a PPM modulator, an input word consisting of several bits is converted into the position of a pulse within a frame, as shown in Figure 2.1. The frame with duration T_{frame} is divided into L slots. Only one of these slots contains an optical pulse of duration T_{slot}. Since there are L possible pulse positions, the number of information bits represented by one pulse is $log_2(L)$. Therefore the bit rate is given as

$$R_b = \frac{Log_2(L)}{T_{frame}}. \tag{2.1}$$

Like in x-OOK, the pulse width can equal the slot duration, or be smaller. Therefore, their width is given by $T_{pulse} = x \cdot T_{slot}$, with $0 < x \leq 1$ [17]. The result is called x-pulse PPM. The height of the pulses is normalized such that the average current through the receiver photodiode is i_{avg}. Since the information is represented by the position of a pulse, a timing reference has to be determined before data demodulation begins. Therefore PPM receivers operate synchronously [17]. An example of an x-Pulse PPM signal is given in Figure 2.2.

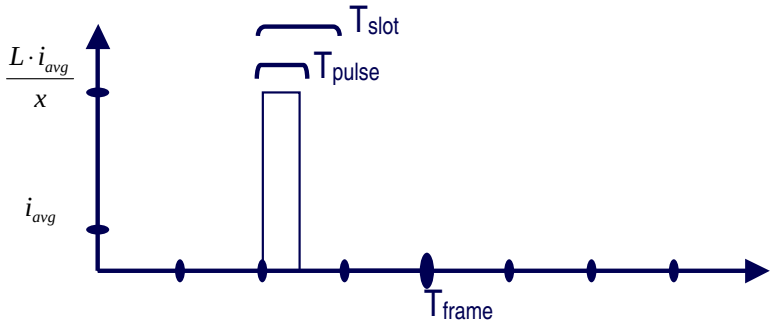

FIGURE 2.2: A PPM signal with L = 4 and x = $\frac{1}{2}$ [17]

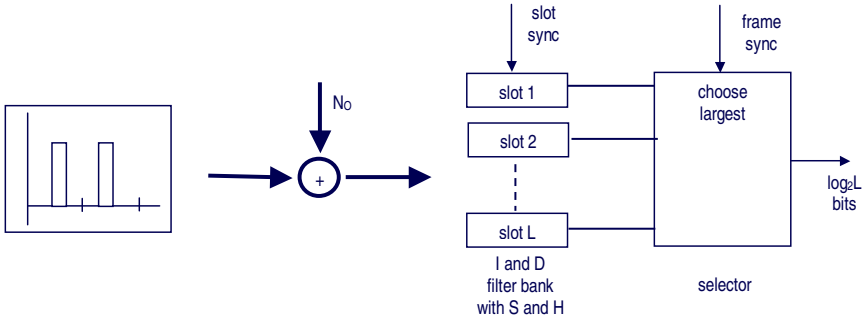

FIGURE 2.3: Block Diagram of a Maximum Likelihood PPM Demodulator [17]

The principle of demodulation is illustrated in Figure 2.3. The slot with the most electrical charge is found to be the one where the original optical pulse occurred. This principle is known as the maximum-likelihood demodulation principle since it determines the most probable pulse position.

PPM offers good immunity to low-frequency optical interference compared to other baseband schemes because the PPM spectrum drops to zero at DC. Another advantage of PPM is it's simple and entirely digital transmitter. Further, it allows for flexible tradeoff between bandwidth and power by choosing the appropriate pulse width and the number of slots per frame.

A more efficient low complexity implementation of a PPM demodulator would consist of only one filter (I&D) and one comparator [17]. This demodulator will require some additional control logic and memory as shown in Figure 2.4.

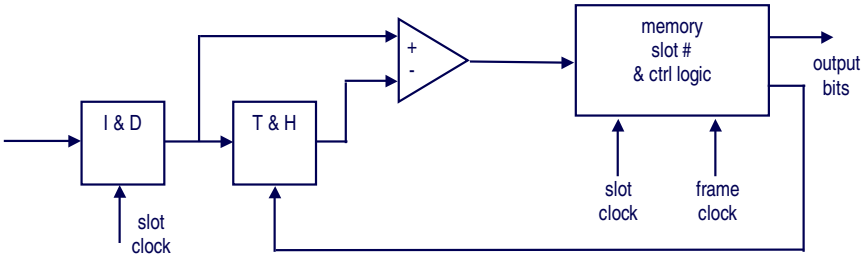

FIGURE 2.4: Block Diagram of an Efficient PPM Demodulator [17]

The I&D block and track and hold (T&H) block can be implemented with a CMOS switch and a capacitor. The T&H will only be loaded by the CMOS switch if the output of the I&D is larger than the previously stored value. The comparator will be a standard comparator with hysteresis, and the memory and control logic can be implemented in the digital portion of the modem in an FPGA.

PPM Synchronization

One of the most difficult problems to solve is synchronization in the receiver. This problem becomes even more difficult in PPM based systems due to the additional digital timing requirements; both slot synchronization and frame synchronization must be determined. Synchronization must be recovered from a single PPM signal in an unidirectional PPM uplink. There are two types of synchronization: spectral based and temporal based. It is recommended to use a spectral based timing recovery method for slot synchronization and a temporal one for frame synchronization. [17]

In the case where one would want multiple remotes, a TDMA network can be implemented. Each sensor would be assigned a particular time slot by a central hub down-link.

For the synchronization used in this system the following flow will be established: first the slot clock will be recovered and then the frame clock will be developed based on the slot clock timing. This recovery scheme is illustrated in Figure 2.5.

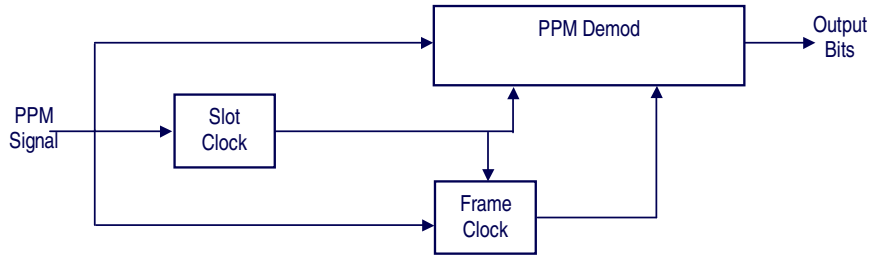

FIGURE 2.5: Basic Synchronization Architecture For a PPM Receiver [17]

PPM Slot Synchronization

The standard full-pulse PPM spectrum is continuous, so the use of a PLL-alone based synchronization will not work due to the inability of the phase detector to lock [17]. Our requirement is to recover the clock phase in every slot at the PPM slot frequency. By preprocessing the PPM signal, a discrete component can be introduced at the slot frequency, thereby giving the PLL phase detector a frequency to lock onto. There are three full-pulse PPM preprocessing options. The first two are nonlinear filtering and edge detection in the receiver, neither of which will work for low-power high-noise level systems. Edge detection can be accomplished by EXORing the PPM signal with a delayed version of itself, thus revealing impulses at every edge.

> This is particularly useful in a system employing 2-PPM, for which an edge-detector alone can be used to recover the slot clock. The spectrum of either method contains a component at the slot frequency. Unfortunately, all these methods require the edge of the PPM pulse to be recognized. In the presence of strong noise this is impossible and reliable demodulation is no longer possible. Therefore, these methods are not recommended for low power systems in the presence of strong noise [17].

The aerospace environment may be sheltered from most noise sources, therefore the edge detector may work and could possibly be the method with the lowest complexity.

Basically, the only way to recover the slot clock for a high noise or low signal level system is to introduce a discrete slot frequency component before the noise enters

the system. This is the third method used for full-pulse PPM, and is performed in the transmitter by use of preprocessing.

The most convenient way to use preprocessing in the transmitter is to use x-pulse PPM modulation [17]. For x-pulse PPM modulation, the pulse duration is less than the slot duration. The slot clock can be recovered by extracting the δ-impulses, which occur at the harmonics of the slot frequency. The discrete part of the spectrum is extracted from the PPM signal by using a filter. The resulting signal contains a pulse in every time slot. The height of these pulses equals $1/L$ times the original PPM height, where L is the number of PPM slots [17]. An added bonus to this filtering scheme is the elimination of most of the noise which causes jitter. Instead of a filter, a Phase Lock Loop could be used to recover the necessary timing.

Frame Synchronization

If frame synchronization has not been correctly established PPM frame errors will occur. These errors can be used to perform digital frame synchronization in the time domain. The PPM frame structure only allows one PPM pulse per frame. If the number of pulses encountered in any frame is not one, a frame error has occurred and must be corrected for. If no noise is present it is possible to get zero, one, or two PPM pulses in one frame, where one corresponds to the correct frame timing and 0 or 2 means that a frame timing error has occurred.

A method to recover the frame timing is to start dividing down the slot clock by L and then count the number of pulses in each frame. One pulse per frame corresponds to no frame errors. If a frame error is encountered, delay the frame pulse by one slot clock and test for frame errors again. These steps are repeated until there is only one pulse in each frame. This time-based method is sub-optimal due to the fact that not all timing and frame-error information are used.

The probability of a frame error is given by [17]

$$P_{fe}(s) = P(p_s = 0) + P(p_s = 2) \tag{2.2}$$

where p_s is the number of pulses found within a frame and s is the PPM frame shift in the case of an error. It follows that

$$P(p_s = 0) = P(p_s = 2) = (s/L) \cdot (1 - s/L) \tag{2.3}$$

$$P(p_s = 1) = (s/L)^2 + (1 - s/L)^2. \tag{2.4}$$

Considering the effects of noise, any number of frame pulses can occur within an erroneous frame or, for that matter, a correctly synchronized frame. Thus, averaging must be incorporated to avoid false PPM errors. The frame error probability with averaging can be expressed as

$$P_{fe} = 1 - ((s/L)^{n+1} + (1 - s/L)^{n+1}) \tag{2.5}$$

$$P_{nosync} = (1/L)^{n+1} + (1 - 1/L)^{n+1} \tag{2.6}$$

where n is the number of frames averaged over.

Once properly synchronized, noise could cause frame errors. Since the noise is known to be independent, frame errors will also be independent. Therefore, the number of frame errors satisfies a binomial distribution. The probability that k errors occur is given by

$$P(x_0 \geq k) = \binom{n}{k} \cdot P_{fe}^k \cdot (1 - P_{fe})^{n-k}. \tag{2.7}$$

Minimum averaging length (n_{min}) should be 100 for high noise levels and 10 for lower noise levels [17].

2.1.3. DPPM

An even more efficient form of PPM is differential PPM. In this modulation scheme the time between pulses is variable, and this variable length contains the information. In a more practical sense, the number of zeros between adjacent pulses maps to a symbol.

The advantage of this scheme is that the receiver does not require symbol synchronization. Table 2.1 gives the re-mapping for 4-DPPM from 2-bit binary words.

2-bit Binary Word	DPPM Mapping
00	1
01	01
10	001
11	0001

TABLE 2.1: 4-DPPM Mapping

Equations (2.8) and (2.9) show that DPPM is more bandwidth and power efficient than PPM [6]. The bandwidth and power required between 16-DPPM and 4-PPM are related to each as:

$$BW_{16-DPPM} = BW_{4-PPM} \tag{2.8}$$

$$P_{16-DPPM} = \frac{1}{2} \cdot P_{4-PPM} \tag{2.9}$$

2.2. Optical Components

2.2.1. Optical Sources

In optical systems, optic beams generated by light sources carry the information. Laser diodes and light-emitting diodes are the most common optic sources. Their small size and low power are compatible with modern solid state electronics [18]. In the majority of optical communication systems, information is put onto the beam by modulating the source input current.

Light Emitting Diode

Due to its moderate bandwidth and ease of use, LEDs are a good choice for the prototype system built in this thesis.

Laser Diode

Laser diodes (LD) are known to have the best power efficiency and largest modulation bandwidth, but they have the narrowest beamwidth and therefore are inappropriate for diffuse NLOS communication.

2.2.2. Optical Detectors

> There are two distinct photo detection mechanisms. The first is the external photoelectric effect, in which electrons are freed from the surface of a metal by the energy absorbed from an incident stream of photons [18]. The vacuum photodiode and the photomultiplier tube are based on this effect. A second group of detectors are semi-conductor junction devices in which free charge carriers (electrons and holes) are generated by absorbing incoming photons. This mechanism is sometimes called internal photoelectric effect [18].

Photodiodes

There are three basic types of semi-conductor photodiodes: pn junction photodiode, PIN photodiode, and avalanche photodiode. The material makeup of the photodiode is determined by the wavelength of the light that the receiver is attempting to detect. Different materials, such as Si or GaAs, are sensitive to different wavelengths of light, thus determining the target wavelength of the photodiode it makes up.

Avalanche Photodiodes

Avalanche Photodiodes (APDs) are silicon photodiodes featuring an internal gain. As with conventional photodiodes, absorption of incoming photons creates electron-hole

pairs, also known as carriers. Because of an APD's internal structure and a much higher reverse bias voltage, a strong internal electric field accelerates the carriers, and these carriers then produce secondary electron-hole pairs by the process of impact ionization. A standard PIN photodiode has unity gain, while the gain of an APD can be up to several hundred. An APD's greatest advantage over traditional photodiodes is the improved Signal-to-Noise (SNR) ratio.

When the level of ambient radiation is small or non-existent, Avalanche Photodiodes (APD) can be very useful. In the APD, current amplification is obtained by means of avalanche multiplication of the photon-generated carriers. Because of this amplification, the relative influence of noise due to the receiver amplifier on the SNR can be reduced. However, the APD amplification mechanism also introduces some excess noise, because it is a random process. Due to avalanche multiplication, the photocurrent is amplified by a factor of A, which is the mean avalanche multiplication factor. This factor can be tuned by adjusting the reverse bias voltage of the photodiode. As a result, the influence of the noise on the preamplifier is reduced by a factor of A^2. On the other hand, the photon detection process is increased by an excess noise factor of $\sqrt{A}$. The high-frequency pre-amp noise can be reduced by means of an APD, at the cost of an increased noise level at lower frequencies [2]. APD devices suffer from saturation effects at high irradiation levels. They also are more costly and require high operating voltages, and hence are predominantly used in specialized systems where performance is key [17]. These issues should be considered when selecting a detector .

2.3. Device Physics

In this section we will discuss the physics of two different devices, a light emitting diode (LED) and a light absorbing diode.

There are two main types of semi-conduction material, one where the majority carriers are electrons known as n-type and the other is where the majority carriers are

holes (absence of an electron) known as p-type. A light emitting diode is a pn junction that emits light when forward biased. Forward biasing is where there is a positive or higher potential on the p-type material and a negative or lower potential on the n-type material. N-type material is silicon mixed with phosphorus, this mixture is referred to as doping for semi-conductors. The p-type material is doped with boron. Undoped Silicon does has very few carriers and therefore will not conduct well when it is bonded to itself. So one must inject silicon with some type of doping material, such as phosphorus or boron to allow for more carriers. These second compounds disturb the perfect structure of silicon and leave an extra electron or hole in the valence band. The level of doping determines the resistivity or conductivity of the material. The higher the level of doping in a material the lower the resistance or higher the conductance [19].

2.3.1. Light Emitting Diode

An LED emits light by converting electrical potential into optical power. This conversion of electrical energy into light is known as electroluminescence. In some semi-conducting materials, free electrons in the conduction band can recombine with holes in the valence band and release a photon in the process. A bias voltage is applied to either side of a semi-conductor. This introduction of additional energy allows un-bonded electrons in the valence band to move to the conduction band, thereby leaving a hole in the valence band. The bandgap energy needed for this process depends on the type of semi-conducting material. Each semi-conducting material has a unique band gap energy which corresponds to a particular wavelength or color of light. One common semi-conducting material used is Gallium-Aluminium-Arsenide (GaAlAs) which has a bandgap energy of 1.48 eV (electron volts) and emits light with a center wavelength of 880 nm (nanometers).

Table 2.2 presents some common semi-conductor materials with their respective wavelength and bandgap energy.

Semi-Conductor	Wavelength (um)	Bandgap Energy (eV)	Color
GaP	0.520	2.4	Green
SiC	0.480	2.6	Blue
GaAs	0.900	1.4	IR
GaAlAs	0.8-0.9	1.4-1.55	IR
InGaAs	1.0-1.3	0.95-1.24	IR
InGaAsP	0.9-1.7	0.73-1.35	IR

TABLE 2.2: Radiant Wavelengths of Different Semi-Conductor Materials

2.3.2. Light Absorbing Diode

The light absorbing diode is commonly referred to as a photodiode or photo detector (PD). A silicon photodiode is a solid-state device that converts light into electric current. When light is absorbed in the active area of a pn device, an electron-hole pair is formed. The electrons pass to the n-region and the holes to the p-region. The migration of electrons and holes to their respective region is called the photovoltaic effect and this results in a current generated by light. The semi-conducting material is quite selective on what kind of photon is absorbed. It takes a photon of the right energy level to send an electron from the valence band to the conduction band. Unlike LEDs, which are forward biased, photodiodes are reverse biased.

Silicon photodiodes are constructed from a single crystal silicon wafer, similar to those used in the manufacturing of integrated circuits. The major difference is that photodiodes require higher purity silicon. The purity of silicon is directly related to its resistivity, with higher resistivity indicating purer silicon. Typical resistivities range from 10 Ω-cm to 10,000 Ω-cm. A cross section of a typical silicon photodiode is shown in Figure 2.6. N-type silicon is the starting material. A thin p-layer is formed on the

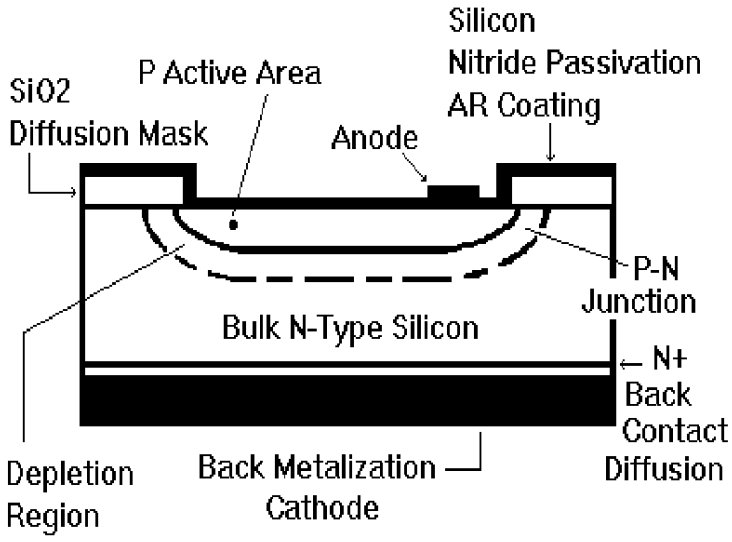

FIGURE 2.6: PN-Diode Cross-Section [19]

front surface of the device by thermal diffusion or ion implantation of the appropriate doping material (boron). The interface between the p-layer and the n-layer is known as a pn junction. Small metal contacts are applied to the front surface of the device and the entire back is coated with a contact metal [19]. The back contact is the cathode and the front contact is the anode. The active area is coated with either silicon nitride, silicon monoxide, or silicon dioxide to serve as an anti-reflection (AR) coating and also for protection [19]. The thickness of this coating is optimized for a particular irradiation wavelength. For example, it might be desirable to enhance its response to the 532 nm range of the spectrum while rejecting 880 nm.

Photodiode junctions are unusual because the top p-layer is very thin. The thickness of the P-layer is determined by the wavelength of the light to be detected. Near the pn junction the silicon becomes depleted of electrical charges. This is known as the depletion region. The depth of the depletion region can be varied by applying a reverse bias voltage across the junction. When the depletion region reaches the back of the diode the photodiode is said to be fully depleted [19]. The depletion region is important to photodiode performance since most of the sensitivity to radiation originates here. The

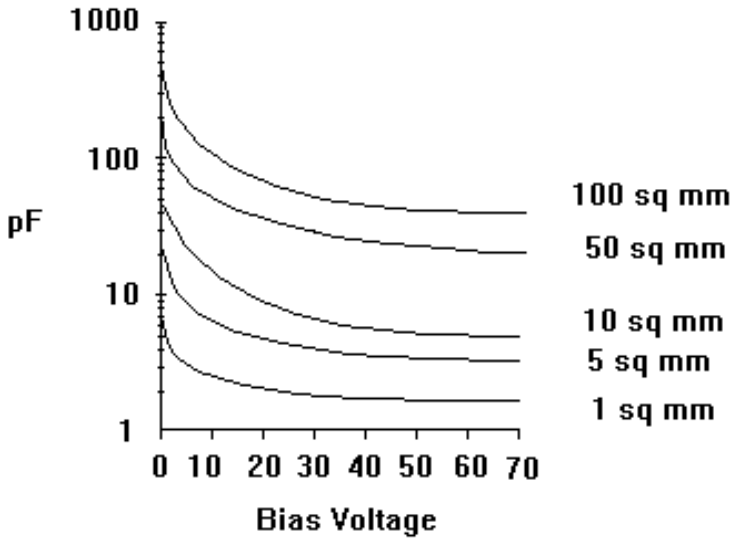

FIGURE 2.7: Bias Voltage vs. Capacitance For Different Photodiode areas [19]

capacitance of the pn junction depends on the thickness of this variable depletion region. Increasing the bias voltage increases the depth of this region and lowers the capacitance until the fully depleted condition is achieved. Junction capacitance is also a function of the resistivity of silicon used and size of the active area. The relationship between junction capacitance, bias voltage and area is shown in Figure 2.7 [19].

Silicon photodiodes are most useful as current generators but can be used as a voltage source. The short circuit current (I_{sc}) is a linear function of the irradiance over a very wide range [19]. When a reverse bias is applied some current will flow without illumination. This current is called the dark current and is usually specified for each device.

A photodiode has two terminals, a cathode and an anode. When the anode is positive it has a low forward resistance, and when the anode is negative it has a high reverse resistance. Normal biased operation of most photodiodes calls for negative biasing the active area of the device, which is the anode, or positive biasing the backside of the device, which is the cathode. In the photovoltaic, photoconductive, and zero bias modes the generated current or voltage is in the diodes forward direction. Therefore,

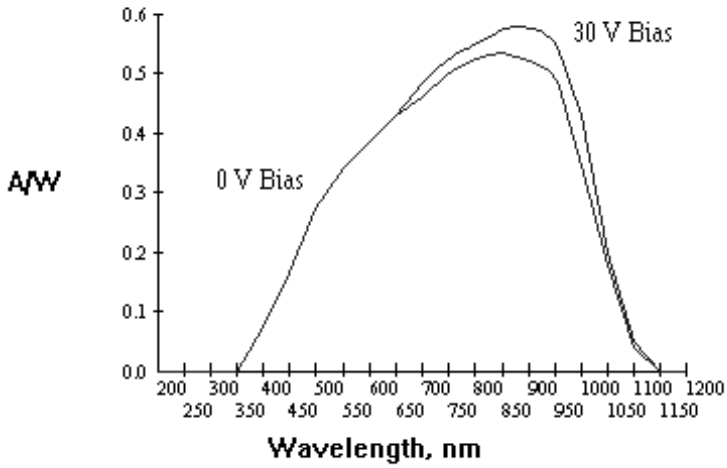

FIGURE 2.8: Diode Responsivity vs. Wavelength For Two Bias Conditions [19]

the generated polarity is opposite of the reverse bias polarity.

The measure of sensitivity or responsivity of a photodiode is the ratio of radiant energy (watts) incident on the photodiode to the photocurrent output (amps). A typical responsivity curve that shows A/W as a function of wavelength is given in Figure 2.8 for two bias conditions.

Quantum efficiency (QE) is the ratio of photo-carriers generated to photons incident on the diode and is usually presented as a percentage. The QE is the ability of a photodiode to convert light energy to electrical energy. Responsivity can be calculated from quantum efficiency (η) using the following equation

$$R = \frac{\eta q}{h\nu} \tag{2.10}$$

where q is the charge of an electron ($1.602 \cdot 10^{-19} C$), h is Planck's constant ($6.626 \cdot 10^{-34} Js$), and ν is the frequency of the carrier.

As can be seen from Figure 2.8 Silicon has a limited range of wavelengths that it will respond to. Above 1100nm, Silicon will behave transparent and below 300nm, UV will be absorbed near the surface of the Silicon and not produce any photocarriers.

Another variable that must be analyzed is the effect of temperature on a photodiode. As temperature changes, the photodiode quantum efficiency and dark current

will be affected. At higher temperatures the quantum efficiency in the IR region will be higher and in the UV region the QE will be lower. Higher temperatures also cause exponential increases in the number of thermally excited electron-hole pairs, resulting in an increase of dark current [19].

2.4. Comparison of RF and Optical Communication Systems

Wireless infrared communication systems possess significant advantages over radio systems in certain environments, including this metal enclosed application [2]. First, the infrared spectral region offers a virtually unlimited bandwidth that is unregulated worldwide [1]. For example, there is over 200THz of bandwidth available in the range of 700-1500 nm wavelength. Propagation of infrared is similar to visible light. Both types of light penetrate through glass, but not through walls or other opaque materials [1]. Thus, infrared transmission is confined to the enclosure in which it originates. The design of secure transmission against eavesdropping and jamming is easily accomplished exploiting this property.

If the LOS path between transmitter and receiver is blocked by an opaque barrier, connections can only be realized via reflections. Since walls typically reflect 65 to 85 percent of the incoming light in a diffuse manner, non-LOS transmission should be possible [27]. This brings to light the next advantage, the inherent spatial diversity of optical communication systems. Since the wavelength of light is several orders of magnitude smaller than the photodiode area, spatial diversity is inherent. One of the major problems in wireless communication is what is known as multipath fading. Fading is a byproduct of the destructive interference caused by multiple paths incident on the receiver. This built-in property in optical systems solves the time varying fading issue, where in RF systems much design effort and materials must go to solving this problem. Therefore the design of infrared systems is simplified and their operational reliability is

increased.

Both mediums suffer from in-band interference, such as microwave ovens for RF and fluorescent or natural light for IR. Each system must be designed to combat these interferers. For the enclosure being dealt with in this thesis, it is assumed that no ambient light is present. The primary source of noise for this optical system will be thermal noise in the receiver.

The primary disadvantage of optical communication systems is it's limited range, particularly when no good path can be found [2]. Infrared is also susceptible to shadowing and the square-law phenomenon. The square-law phenomenon states that the received electrical power is proportional to the square of the received optical power. This is due to the optical power exciting a current and not power in the photodiode receiver. The advantage is that if the optical power in the transmitter is increased by 3dB, the received electrical power increases by 6dB. The flip-side is that if the path loss is doubled the received electrical power decreases by 6dB.

The design and manufacturing of an optical system frontend is much less complex than building its RF counterpart. Both RF and optical systems suffer from multipath dispersion, which causes intersymbol interference, but only the RF system experiences true multipath fading. A summary of the main differences between IR and RF systems are presented in Table 2.3.

2.4.1. Link Analysis Comparison Between IR and RF

A general link budget comparison will be performed between a common IR system and an RF system. The IR system used will be the one used for testing in this thesis and the RF system will be a 2.4GHz evaluation kit (ML2724-EVK) provided by Microlinear Corporation. From Table 2.4, which details this analysis, it is clear that it is difficult for an optical system to compete with its radio counterpart. There must be other motiva-

Property	Optical	Radio
Multipath Fading	No	Yes
Multipath Dispersion	Yes	Yes
Source of Bandwidth Limitation	High photodiode capacitance, Multipath dispersion	Regulatory
Source of Dominant Noise	Ambient Background Light	Interference from other users
Security	High	Low
Range	Low	High
Front End Complexity	Low	High

TABLE 2.3: Properties of Optical and Radio Channels. [13]

tions, such as low complexity, low cost, high data-rate, or small size, to justify the use of an optical communication system. The path loss figures for IR systems is calculated from the Ceiling Bounce Model, given in Equation (1.8). The path loss for RF systems is calculated from Friis equation (2.11) and is given as

$$P_{LossRatio} = \frac{P_R}{P_T} = \frac{G_A \cdot G_B}{(4\pi \frac{R}{\lambda})^2} \tag{2.11}$$

where G_A and G_B are the antenna gains for monopole antennas and R is the link distance.

Item	IR ($880nm$)	RF (2.4GHz)
Transmit Current	$100mA$	$100mA$
Transmit Power	$14.77dBm(30mW)$	$15.77dBm(32mW)$
Path Loss (1 meter)	$-50dB$	$-41dB$
Received Power	$-35.23dBm$	$-25.23dBm$
Rx Sensitivity ($BER = 10^{-3}$)	$-65dBm$	$-85dBm$
Margin	$29.77dB$	$59.77dB$

TABLE 2.4: IR versus RF link budget

CHAPTER 3. SYSTEM ARCHITECTURE

Based on the theory presented in Chapter 2, a possible system architecture is proposed in this chapter.

3.1. Prototype

3.1.1. System Requirements

The proposed system must be capable of a bit error rate of 10^{-5} at a distance of 1 meter while maintaining low power and a data rate of at least 100Kbps. The low power requirement states that the transmitter or receiver current cannot exceed an average of 50mA. The design should be capable of a final form factor of less than one inch cubed. A summary of these parameters is presented in Table 3.1.

Parameter	Value	Unit
Tx/Rx Current (Avg.)	≤ 50	mA
Link Distance	≥ 1	$Meters$
BER	$\leq 10^{-5}$	-
Data Rate	≥ 100	$Kbps$
Dimensions	≤ 1	$inch^3$

TABLE 3.1: System Specifications

3.1.2. System Specification

The prototype system block diagram is presented in Figure 3.1. For ease of reproducibility and manufacturing it is a fairly simple design. This prototype consists of three main parts: the transmitter, the channel, and the receiver. The transmitter is composed of a data source, a modulator, and an infrared analog front-end. The channel will be a metal enclosure with varying surface types. The receiver is broken down into an infrared receiver, demodulator, and data sink.

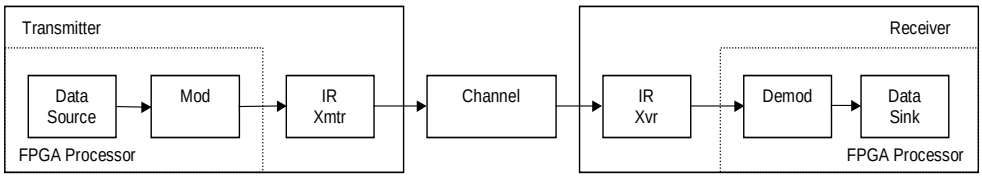

FIGURE 3.1: Block Diagram of the Infrared Communication System

3.2. Transmitter

The transmitter is broken down into two parts, the analog front-end and the digital baseband.

3.2.1. Analog Front-End

The analog front-end for an optical system is quite simple. It consists of only a switch, an amplifier, and an optical source. A bipolar junction transistor (BJT) with a resistor will be used to implement the switch and current amplifier. Due to the diffuse nature of this system an LED will be used as the optical source because of its wide beam width.

The infrared transmitter front-end consists of a single LED operating in the 700-1000 nm range. LEDs offer the advantage of allowing for a simple control circuit and modulation bandwidths up to 10MHz at 20% efficiency [1]. The LED used for this prototype was supplied by Opto-Diode and operates in the range of 880 nm as shown in Figure 3.2. The specifications for this LED are provided in Table 3.2.

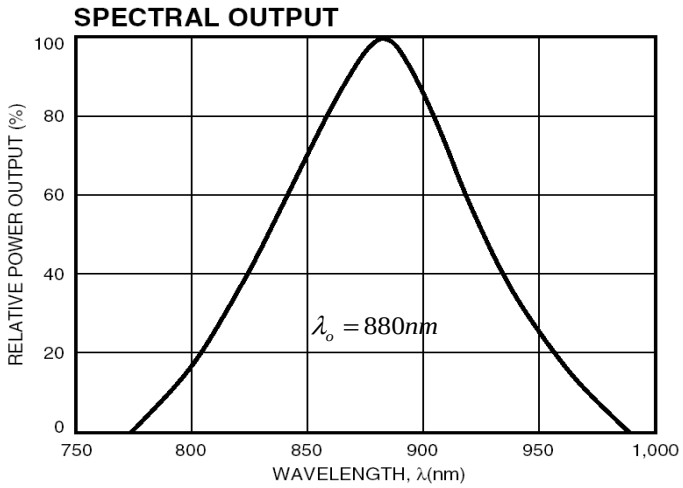

FIGURE 3.2: Spectrum of 880 nm LED [25]

Using Figure 3.3 the transmit power of the diode can be determined. This figure presents the optical power to electric current efficiency and was provided by Opto-Diode. An average current of 50mA will produce 15-20mW of average optical power.

The schematic for the transmitter front-end is presented in Figure 3.4.

3.2.2. Baseband Transmitter

The base band portion of the transmitter will consist of a binary random number generator and a digital modulator. To implement a random number generator a linear

Parameter	Typical	Units
Power Output @ 100mA	30	mW
Beam Angle @ -3 dB	90	$degrees$
Wavelength	880	nm
Spectral Bandwidth @ -3 dB	80	nm
Forward Voltage	1.6	$Volts$
Reverse Breakdown Voltage	30	$Volts$
Power Output @ 100mA	30	mW
Response Time (Rise/Fall Time)	0.5	us
Capacitance	17	pF

TABLE 3.2: OP-880E LED Specifications

feedback shift register (LFSR) will be used. A linear feedback shift register is typically used in any digital system that relies on pseudorandom bit sequences (PRBS), with applications ranging from cryptography and bit-error-rate measurements, to wireless communication systems employing spread spectrum techniques [21].

> Pseudorandom sequences are generated using a binary shift register with taps that are modulo-2 added together and fed back to the register's input. The name commonly used for this simple circuit is linear feedback shift register, or LFSR. The type of sequence generated by an LFSR is called a linear recursive sequence, or LRS [21].

Linear feedback shift registers can be implemented in one of two ways, Fibonacci or Galois implementation. The Fibonacci implementation consists of a shift register in which a binary weighted modulo-2 sum of the taps is fed back to the input (see Figure 3.5). The Galois implementation consists of a shift register, the contents of which are modified at each step by a binary weighted value of the register output [21]. The all-zero

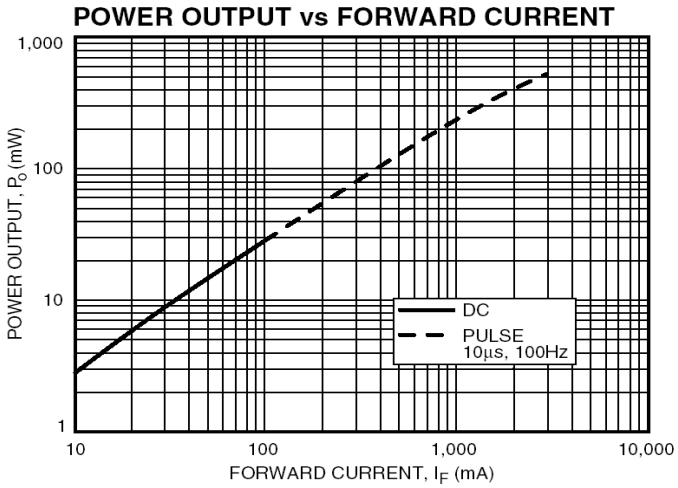

FIGURE 3.3: Optical Power vs. Electric Current for OD-880E (Courtesy of Opto Diode)

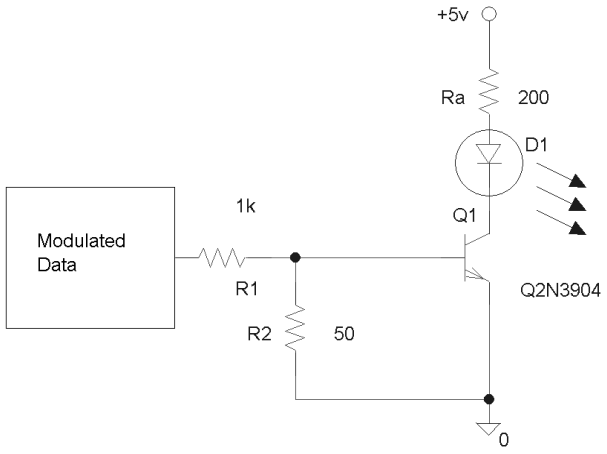

FIGURE 3.4: Optical Front-End Schematic of the Transmitter

condition is avoided since that would lock up the LFSR and set the output to only zeros.

The data source generation and modulation are performed in an Altera FPGA. The source data is a pseudo random bit stream (PRBS) generated by a linear feedback shift register (LFSR). The PRBS data is generated by Equation (3.1), a PN9 sequence generator, which is a standard pseudo-noise (PN) generator. A schematic of a PN9 generator is presented in Figure 3.5. This generator is broken down into two parts, a

shift register and a feedback XOR-gate used for modulo-2 addition

$$G(X) = X^5 + X^9. \tag{3.1}$$

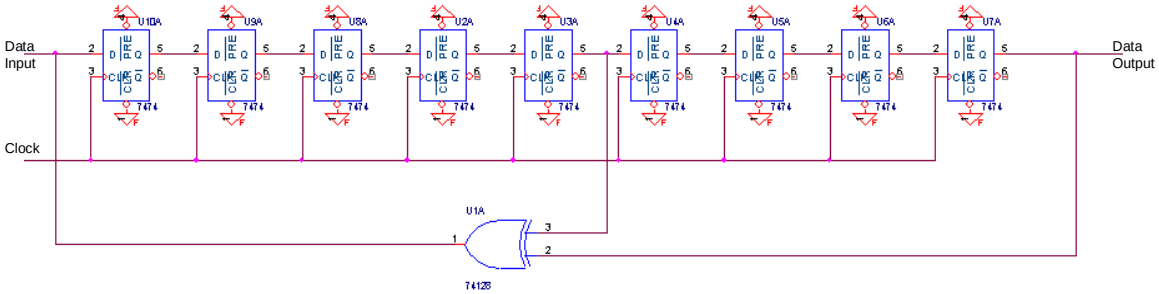

FIGURE 3.5: PN9 Schematics

The modulator is implemented with a look-up table that maps from 2-level NRZ digital data to the chosen modulation. For NRZ-OOK, this step is bypassed due to the digital data source and NRZ-OOK being the same. For RZ-OOK, a D-type flip-flop with enable is used to convert from NRZ to a 50% duty cycle RZ. More details can be found in Figure 3.6. In the case of PPM, a re-mapping would be necessary.

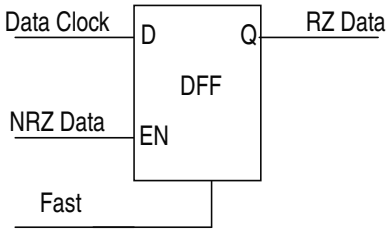

FIGURE 3.6: 50%-duty-cycle return-to-zero data encoder

3.3. Receiver

The receiver is also broken down into two parts, the analog front-end and the digital baseband.

3.3.1. Analog Front-End

A Si PIN photodiode will be used for the receiver. The performance is close to ideal when considering bandwidth, noise performance and responsivity. Since the receiver sensitivity increases with detector area, a large photodiode should be used. The capacitance of these photodiodes equals approximately $3-5pF/mm^2$, so the photodiode capacitance can be rather large. This capacitance increases the front-end RC-time constant, which decreases the achievable data-rate and increases the noise. Optical wireless receiver designs must be tolerant of very high input capacitances due to photodiodes requiring such large active areas. The best approach is to combine a transimpedance amplifier with bootstrapping techniques, which reduce the effective capacitance of the photodiode.

There are two possible ways to detect the infrared signal: direct detection or coherent detection. Coherent optical detection is not possible in the diffuse aerospace environment due to the frequency and phase information being lost in the propagation process. A block diagram of direct detection is shown in Figure 3.7. There are two kinds of reflection for light: specular, where the angle of reflection equals the angle of incidence; and diffuse, where the reflected wave is scattered in a semi random fashion losing any phase information. Infrared modulation breaks down into three categories; intensity, wavelength (frequency), or polarization (phase) modulation. The IR system will be employing diffuse communication in the metal enclosure with multiple reflections. After the optical signal experiences a reflection, most of the frequency and phase information will be corrupted. This phenomenon will make it difficult, if not impossible, for the detector to extract any frequency or phase information. Therefore, intensity modulation with direct detection (IM/DD) will be used. IM/DD is not severely affected by multiple reflections. For IM, the current in the photodetector is proportional to the received optical signal intensity, which is the original modulated signal.

Direct detection is based on a photon counting method. The current produced

in a photodetector can be broken down into two statistical parts, the mean (Equation (3.2)) and variance (Equation (3.3)) of $i(t)$. Where the mean is the modulated signal of interest and the variance is the noise [20].

$$i_s(t) = i(\bar{t}) = \frac{\eta q}{h\nu} \cdot P_{rcvd} \cdot \int_0^t h_d(\tau) d\tau \qquad (Amps) \tag{3.2}$$

$$i_n^2(t) = vari(t) = \frac{\eta q}{h\nu} \cdot P_{rcvd} \cdot \int_0^t h_d^2(\tau) d\tau \qquad (Amps^2) \tag{3.3}$$

where η is the quantum efficiency of the photodetector, q is the electron charge, h is Planck's constant, and ν is the carrier frequency or frequency of the light source. Taking the Fourier transform of $i_n^2(t)$ yields Equation (3.4)

$$i_n^2(f) = 2qI_{dc} \qquad (Amps^2/Hz). \tag{3.4}$$

Considering bandwidth we get Equation (3.5)

$$I_n^2 = 2qI_{dc}B \qquad (Amps^2). \tag{3.5}$$

The photocurrent produced in a direct detection receiver is given by

$$i_{photo}(t) = i_{DC} = \frac{\eta q}{h\nu} \cdot P_s. \tag{3.6}$$

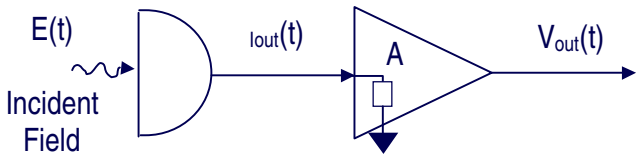

FIGURE 3.7: Direct Detection Receiver

Referring to Equation (3.6), the output of the direct detection receiver is directly proportional to the power in the received field [20]. Thus the output current only responds to power fluctuations in the received field, not the phase, frequency, or polarization of the signal.

Using the output of the direct detection receiver the ultimate signal-to-noise ratio can be determined. The signal portion is the electrical power dissipated in the load resistor due to the DC photocurrent. Therefore, the signal power, Equation (3.7), is equal to the mean-squared photocurrent multiplied by the load resistor.

$$P_{signal} = i_{DC}^2 \cdot R_l = \left(\frac{\eta q}{h\nu} \cdot P_s\right)^2 \cdot R_l \tag{3.7}$$

The electrical power of the shot noise, given by Equation (3.8), is equal to the mean-squared noise current multiplied by the load resistor

$$P_{noise} = i_{noise}^2 \cdot R_l = 2q \cdot i_{DC} \cdot BR_l = 2q \cdot \frac{\eta q}{h\nu} P_s \cdot BR_l. \tag{3.8}$$

Quantum shot noise forms the fundamental limit to the SNR and consequently sets the ultimate sensitivity limit for an optical receiver. The maximum achievable SNR in direct detection optical receivers is given by the ratio of the signal power to the noise power as

$$SNR_{dd} = \left(\frac{P_{signal}}{P_{noise}}\right) = \frac{1}{2} \cdot \frac{\eta}{h\nu \cdot B} \cdot P_{signal} \tag{3.9}$$

where the bandwidth (B) is determined from the bit-rate (R_b) and the number of symbols (L) using the following relation:

$$B = \frac{L}{log_2(L)} \cdot R_b. \tag{3.10}$$

Once the SNR is found, knowing that the noise is independent, white, and Gaussian, the BER can be determined from the error function as

$$BER = Q\Big(\sqrt{0.5L \cdot log_2(L)} \cdot \sqrt{SNR}\Big). \tag{3.11}$$

The front-end consists of a photo-detector and a current amplifier. A silicon photodiode with a bias voltage is used as the photo-detector while the current amplifier is implemented with a BJT transistor. The collector lead is isolated from the +5V power source with a resistor. The schematics for the receiver front-end are presented in Figure 3.8. The DC value at the collector is unknown since the level at which the current amplifier will be turned on is controlled by a pseudo-random current from the photo-detector.

To solve this problem, a carefully selected DC-decoupling capacitor is placed in series with the signal path. The selection of this capacitor must be chosen such that the DC value is filtered out but the AC data signal is allowed to pass. Then a comparator with one input set to ground level is used as a data slicer to convert from an analog signal to a digital signal (1-bit ADC). Since the current amplifier is of the inverting type, another inverter must be placed after the comparator to fully restore the data. Figure 3.8 presents the front-end receiver schematics.

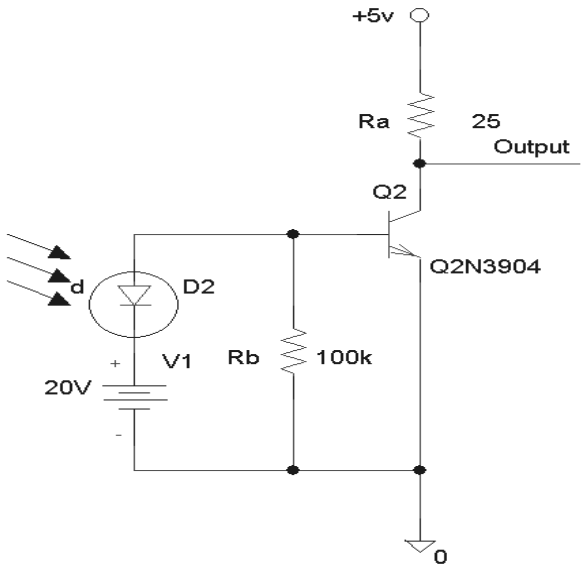

FIGURE 3.8: Optical Front-End Schematic of the Receiver

Infrared Portion

Since the information-carrying signal after the photodiode is a current, the front-end amplifier is either a transimpedance amplifier or a current amplifier. Up to this point, the optical signal coming from the amplifier has been shaped by the channel and all the various circuitry, including the circuit parasitics. These analog pulses must be converted to a digital format consisting of just two levels, VCC and GND. This function is performed with a comparator which is also known as a data-slicer. This operation is most easily performed by removing the DC component and passing the DC decoupled signal

to the first comparator input. The second input to the comparator will be grounded and used as a reference. When the DC decoupled signal dips below reference, the negative comparator rail is used and when it rises above, the positive rail is used. A schematic of these functions is presented in the upper half of the circuit in Figure 3.10.

Non-directed diffuse transmission results in a highly diluted signal irradiance (power per unit area). The poor power efficiency of the link merits the use of a truncated spherical optical concentrator at the receiver. The detector area can be enlarged without increasing the diode capacitance by using an optical lens. This increased photodetector area results in more received power. Maintaining minimum photodiode area permits minimum capacitance, which allows for maximum bandwidth. High PD capacitance is the major obstacle to wideband low-noise pre-amplifier design. The electrical SNR ratio is nearly proportional to the optical gain of the concentrator and is approximately n^2 if the following relationship holds

$$R \geq \frac{nr}{\sqrt{1 - n^2 cos^2 \theta_t}} \tag{3.12}$$

where R is the concentrator radius, n is the index of refraction, r is the detector radius, and θ_t is the FOV angle [13].

To improve the signal-to-noise ratio, an optical filter that would efficiently reject the optical noise is needed in some applications. These filters are made up of a stack of thin dielectric slabs with varying indices of refraction. These thin film filters are useful for creating a narrow-band optical filter. It is recommended to use a spherical shaped filter placed on the concentrator rather than a planner one on the surface of the Si photodiode [20]. The filter should also include an anti-reflection (AR) coating. Thus, functionally, the optical front-end of the receiver branch consists of an optical concentrator, an optical band-pass filter, and a photodiode. The optical front-end must be carefully manufactured with an index-matching compound between each component.

These components change the photodiode area seen by the background light in the

following way:

$$A_{bg} = n^2 T_o A \tag{3.13}$$

where $n^2 T_o$ is the optical gain, n^2 is the gain from the lens, T_o is the peak filter transmission loss, which includes the filter loss and reflection loss, and A is the actual photodiode area.

The detector area seen by the signal can be approximated in the following way:

$$A_{eff} = n^2 T_o A \cdot \cos\psi \tag{3.14}$$

where ψ is the incident angle of the signal on the detector.

3.3.2. Baseband Receiver

The digital section of the receiver will be made up of a demodulator, digital clock recovery circuit, and bit frame comparator. The demodulator will re-map the OOK or PPM information into a digital format suitable for recovering the clock timing information. The BERT compares the received pseudo random sequence with a locally generated one, when a difference is encountered an error counter is incremented. The error detector portion of the unit receives data and clock signals from the baseband portion implemented in an FPGA. The external clock fed in along with data (from the FPGA) generates a reference pattern which is compared with the input data to measure the errors. The reference circuit employs a 9-bit shift register with tapped outputs as per the assigned polynomial code lengths [31]. The length of the pseudo random sequence is $2^9 - 1$.

The FPGA is used to extract the necessary timing information from the data. This is accomplished by using a fast 2-bit shift register to detect rising edges. The signal that is generated by the data edges is used to reset a counter which will output the recovered clock. Since the data rate is known ahead of time, only the phase has to be recovered,

which is done by resetting the counter with the edge signal. The counter will divide down a faster clock to the desired data rate.

Channel

The channel is constructed of a 26AWG tin metal box of dimensions $24 \times 24 \times 26$ inch^3 for diffuse NLOS testing, while the LOS testing was performed in an open air lab environment.

3.4. Diversity

Diversity is implemented in the analog front-end of the transmitter and receiver. The most effective diversity scheme in optical communication links is angular diversity, where transmission and reception is attempted at more than one angle. Figure 3.9, an electrical schematic, shows how the transmitter diversity setup is wired. Physically the LEDS are positioned 90^o apart so that each LED illuminates a 90^o section of the 180^o span. The LED current and power are kept constant between one LED and two LED's, i.e. one LED (1 transmitter) $LED_{current} = 40mA$ and two LED's (2 transmitters) $LED_{current} = 20mA$. The schematics for the transmitter and receiver front-ends with diversity are presented in Figures 3.9 and 3.10.

Figure 3.10 presents the proposed selection diversity setup. Figure 3.8 is represented in each of the PD boxes shown in Figure 3.10.

The specifications for the two types of photo diodes used are provided in Table 3.3. The $100mm^2$ PD has a better dark current because of a better manufacturing process. Under normal circumstances the larger PD would have a larger dark current. Also, the rise-time calculations in this table were calculated using a 50Ω load.

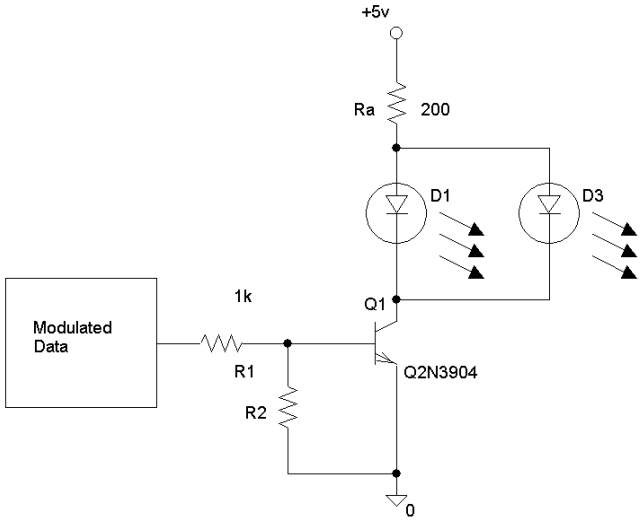

FIGURE 3.9: Optical Front-End Schematic of the Transmitter with Diversity

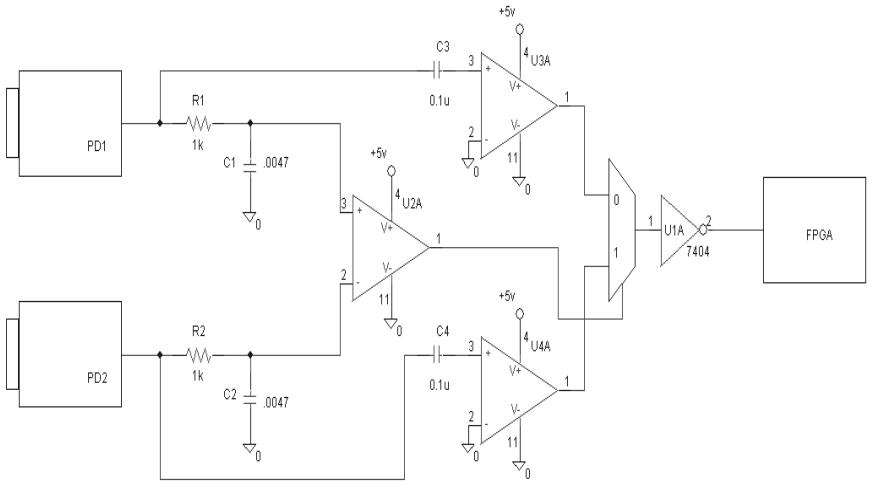

FIGURE 3.10: Receiver Selection Diversity Schematic

Parameter	$OSD100-0A$	$OSD35-3T$	Units
Active Area	100	35	mm^2
Dark Current Max	70	150	nA
NEP @ 880 nm	2.5×10^{-13}	4.8×10^{-13}	$W/\sqrt{Hz}$
Capacitance @ 20V	410	140	pF
Risetime	10	12	ns
Responsivity	0.54	0.61	A/W

TABLE 3.3: Photo Diode Specifications

CHAPTER 4. RESULTS

4.1. Theoretical Analysis

A generalized optical communication link is illustrated in Figure 4.1. Initially the information to be transmitted to the receiver is in an electrical form [20]. The information source modulates the field generated by the optical source. The modulated optical field then propagates through an optical channel. The receiver may perform optical processing on the incoming signal. The optical processing may correspond to a simple optical filter or an optical concentrator (lens) [20]. Once the received field is optically processed it is detected. The photo-detection process generates an electrical signal that varies in response to the modulation present in the received optical field. Electrical signal processing is then used to recover the information that is being transmitted.

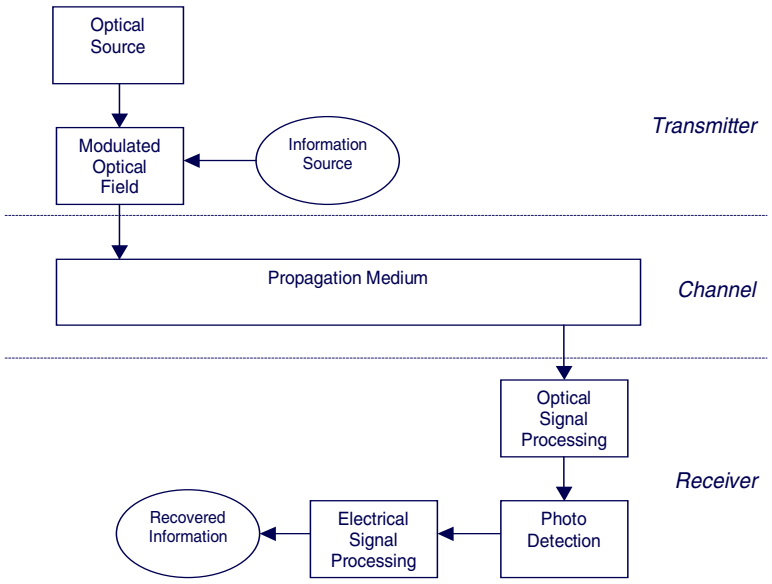

FIGURE 4.1: Generalized Optical Communication Link [20]

4.1.1. Link Budget Analysis

The overall system-level performance of an optical communication link is easily quantified in terms of a system link budget [20]. This is the same technique used in microwave communication links. A link budget provides a convenient tally sheet where a system's performance constraints may be accounted for [20]. Finite transmitter power, modulation imperfections, optical gains and losses, receiver sensitivity, atmospheric losses, and electronic imperfection are all conveniently expressed in terms of their impact on the ultimate communications performance of the link [20].

All link budgets will have at least three entries, one for the transmitter, one for channel, and one for the receiver. The last entry to the link budget analysis is the receiver sensitivity. This sensitivity is the amount of optical signal power that must be present at the receiver to meet the link user's quality of service (QoS) requirements [20]. The difference between the amount of power actually present at the receiver and the receiver sensitivity gives the link margin. Any communication system that desires to maintain a specified QoS will require that a minimum signal-to-noise ratio (SNR) be maintained within the receiver. The receiver sensitivity specification is essentially the amount of optical signal power needed to obtain the SNR required to provide the desired quality-of-service. The exact SNR needed depends on a) the receiver noise statistics; b) type of modulation, detection, and demodulation employed; c) the imperfections in the modulator, photodetector, and demodulator; d) optical nonlinearities; and e) any error correcting coding techniques that may be used [20].

Figure 4.2 illustrates the principal entries in the link budget for an optical communication system. The entries are average transmitter power, modulation losses, transmitter antenna gain, transmitter optical loss, space propagation loss, losses in the channel from scattering attenuation, spatial pointing of tracking loss, receiver antenna gain, receiver optical loss, and receiver sensitivity.

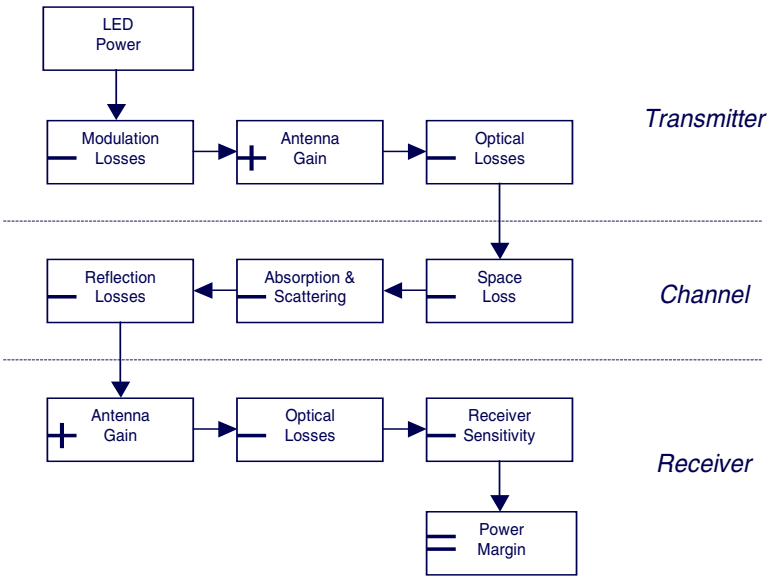

FIGURE 4.2: Components of a Communication System Link Budget ([20]

The antenna gain in this budget is computed using the formula for the ideal gain of a uniformly illuminated circular aperture, and is given as

$$G_a = \left(\frac{\pi D}{\lambda}\right)^2 \tag{4.1}$$

where D is the aperture diameter.

The loss due to light spreading in free-space propagation is given by

$$L_p = \left(\frac{\lambda}{4\pi R}\right)^2 \tag{4.2}$$

where R is the propagation path length in meters.

An example link budget for the optical communication system in this project is presented in Table 4.3.

Receiver Sensitivity Budget

An early system level evaluation of the effects of receiver, channel, and transmitter imperfections is critical in determining the ultimate performance achievable by a communication link [20]. The aspects that cause significant performance degradations must

Link Analysis				
	Item	Value (W)	dB Value	Unit
Transmitter:				
	Average Power	0.1	13.0	dBm
	Optical Loss		-3.0	dB
	Effective Radiated Power		10.0	dBm
Channel:				
	Path Loss	3 meter	-64.0	dB
	Reflection Loss	3 reflections	-2.0	dB
Receiver:				
	Antenna Gain	2cm	4.0	dB
	Angular Diversity	2 Detectors	3.0	dB
	Optical Losses		-3.0	dB
	Received Optical Power	6.30957E-09	-52.0	dBm
	Received Electrical Power (R*Ps)^2 * (Rl)	7.16593E-16	-121.4	dBm
	Noise Power 2q*R*Ps*BW*Rl	2.42E-20	-166.2	dBm
	SNR @ Receiver		44.7	dB
	SNR @ Receiver | Required (BER=10e-6)		7.0	dB
Link Margin:			37.7	

Note: R=0.6A/W, R_L=10kΩ, BW=0.1Mbps, λ=880nm, A_{PD}=35mm^2

FIGURE 4.3: Link Budget for 0.1Mbps Optical Sensor

be identified. There are many types of losses and imperfections in the receiver. The receiver sensitivity budget accounts for these losses. One loss is due to some photons not being absorbed and some being reflected, which is called photo detector noise. Second, there are losses due to various amplification stages, though the first amplifier dominates the bulk of the total amount of noise. The effects of imperfect modulation begin in the transmitter, but appear first in the receiver, therefore they are accounted for there [20]. Some losses will inevitably occur because no modulation scheme is perfect. Within the demodulator and clock recovery subsystems there are additional degradations due to imperfect filter bandwidths and jitter in the recovered clock signal. Figure 4.4 goes through all these calculations for this project.

Receiver Sensitivity				
Item	Value	Photons / Symbol	Power	Unit
NEP (W/Hz^-0.5)	1.90E-13		-127.2	dB
Pmin for SNR =1	1.20E-10		-99.2	dB
NEP*sqrt(BW)				
SNR = 7 => BER = 1e-6			7.0	dB
Ideal Performance	6.02E-10		-92.2	dB
Photons per Bit	6665.51	38.2		dB
Photo Detection Losses:				
Efficiency QE	0.85	0.7		dB
Excess Detector Noise		0.8		dB
Amplifier Losses:				
Noise		0.7		dB
Distortion		0.5		dB
Demodulator Losses				
Imperfect Modulation		1.0		dB
Non-ideal Filter Bandwidth		0.6		dB
Sample Time Jitter and Offset		0.4		dB
Actual Performance Required (photos/sym.)	19716.67	42.9	-87.5	dB
Receiver Degradation		4.7	-57.5	dBm
Received Optical Power			-52.0	dBm
Receiver Sensitivity Margin			5.5	

FIGURE 4.4: Receiver Sensitivity Budget

4.2. Simulation Results

4.2.1. Digital Simulation in MATLAB

Figure 4.5 demonstrates the 6 dB advantage of 4-PPM over OOK modulation. These results have been verified analytically as will as by simulation. The theoretical performance equations are presented in Table 4.1 [2].

Modulation Type	P_e	Bandwidth
On-Off Keying	$Q\left(\sqrt{SNR}\right)$	R_b
OOK RZ-δ	$Q\left(\frac{1}{\sqrt{\delta}} \cdot \sqrt{SNR}\right)$	$\frac{1}{\delta}R_b$
L-PPM	$Q\left(\sqrt{\frac{1}{2}L \cdot log_2(L))}\sqrt{SNR}\right)$	$\frac{L}{Log_2(L)}R_b$

TABLE 4.1: Theoretical Performance Equations of OOK and PPM Modulation [2]

4.2.2. Analog Simulation of Frontend in Spice

One of the key design criteria for a communication system is the data-rate bandwidth which is limited by the rise-time in the receiver front-end. For an optical system the limiting factor for the receiver frequency response arises from the photodiode frequency response. Although a large field of view is desired in the diffuse multipath system, the large photodiode area may also lead to a large capacitance. This capacitance contributes to the frequency response of the photodiode. A circuit diagram (Figure 4.6) and spice simulation (Figures 4.7 and 4.8) have been run to show the effect of the photodiode circuit on a received pulse. It is shown in Figure 4.7 that there is a 1.2us rise time for a 2.5us square pulse. This phenomenon can cause ISI which may lead to poor performance. ISI can be compensated for by equalization or by using a RZ-OOK scheme.

Current source $I1$ represents the optically generated photocurrent in the depletion region of the photodiode. R_j is the junction resistance and represents the differential resistance of the diode. For a high-quality diode operating in the reversed bias mode this resistance is typically greater than 10^6 ohms and can be ignored. C_j is the junction capacitance and arises from the separation of charge in the depletion region. C_b is the bond pad capacitance and L_s is the series inductance due to a wire connecting the cathode of the diode to other circuit components in the system. The series resistance R_s is due to bulk contact resistance, which is the contact of the diode to the circuit board.

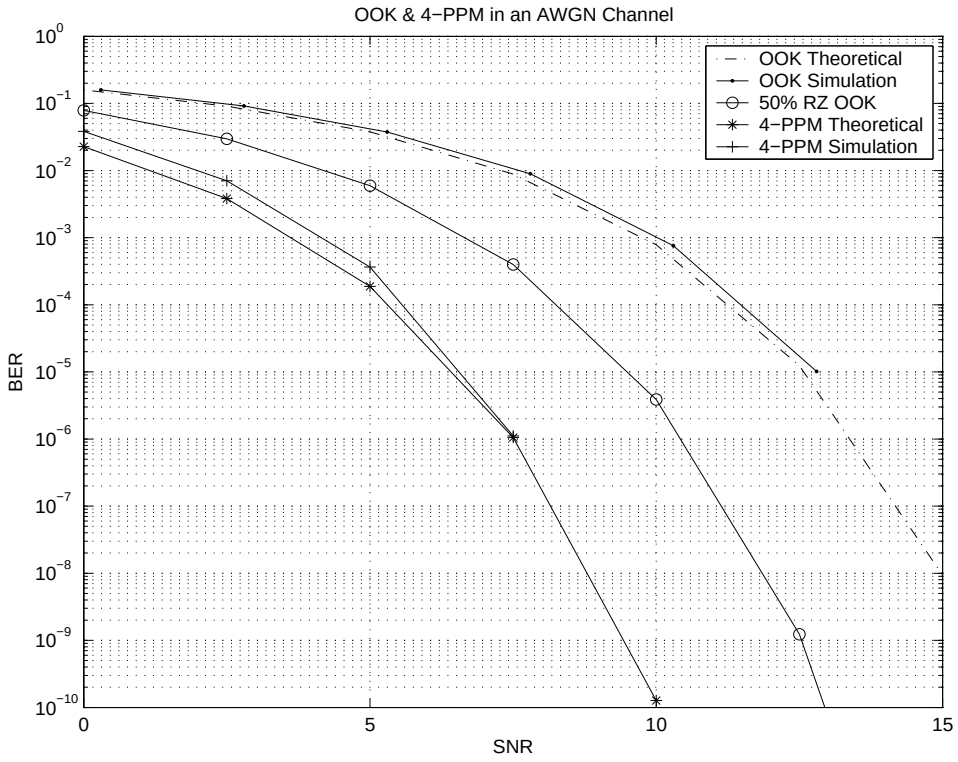

FIGURE 4.5: Simulation with Theoretical Validation for OOK & 4-PPM in an AWGN Channel

C_p is the package or parasitic capacitance due to the packaging of the detector. [24]

From Figure 4.7 it is clear that the received pulse is being reshaped by some type of low pass filter operation. This leads to a slightly attenuated, delayed, and rounded pulse. Taking the the Fourier Transform (64K-points FFT) of the temporal waveform yields the frequency response and reveals the overall communication system bandwidth limitation. The FFT result is presented in Figure 4.8, which shows that the circuit in Figure 4.6 has a 3 dB bandwidth of approximately 200KHz.

For optical systems using a photodiode as the receiver, there is a tradeoff between frequency response and received signal level. The wider the system bandwidth the lower the received signal level at the load resistor. This tradeoff is controlled by the selection of the load resistor. Due to the large propagation path loss in this channel, the signal

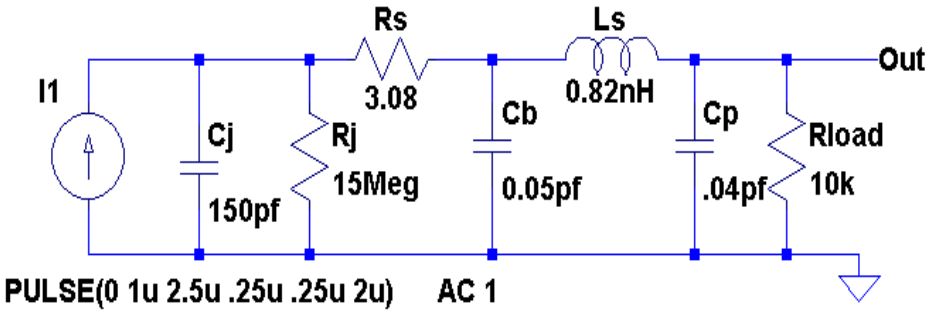

FIGURE 4.6: Photodiode Circuit Model [24]

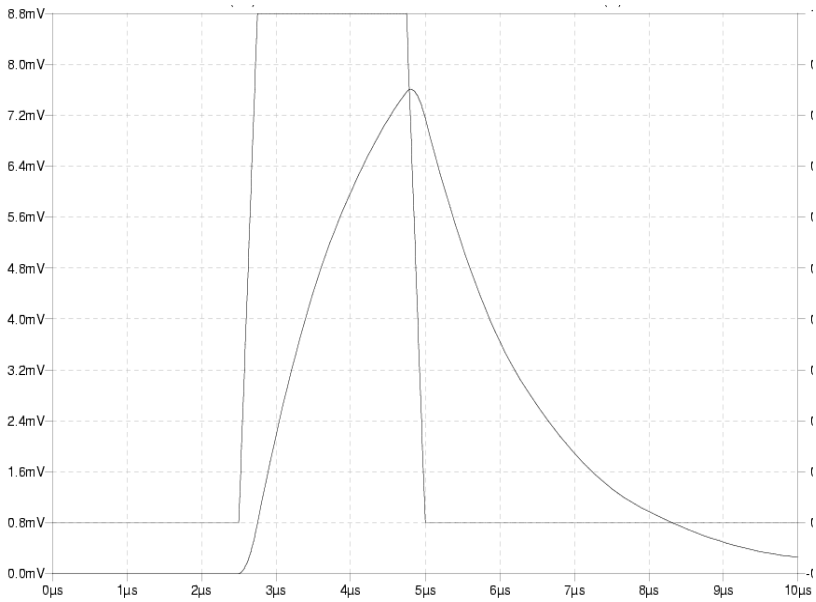

FIGURE 4.7: Photodiode Circuit Temporal Response

level must be maximized in order for the communication link to be reliably established. Thus, the system bandwidth is narrow and is presented in Figure 4.8.

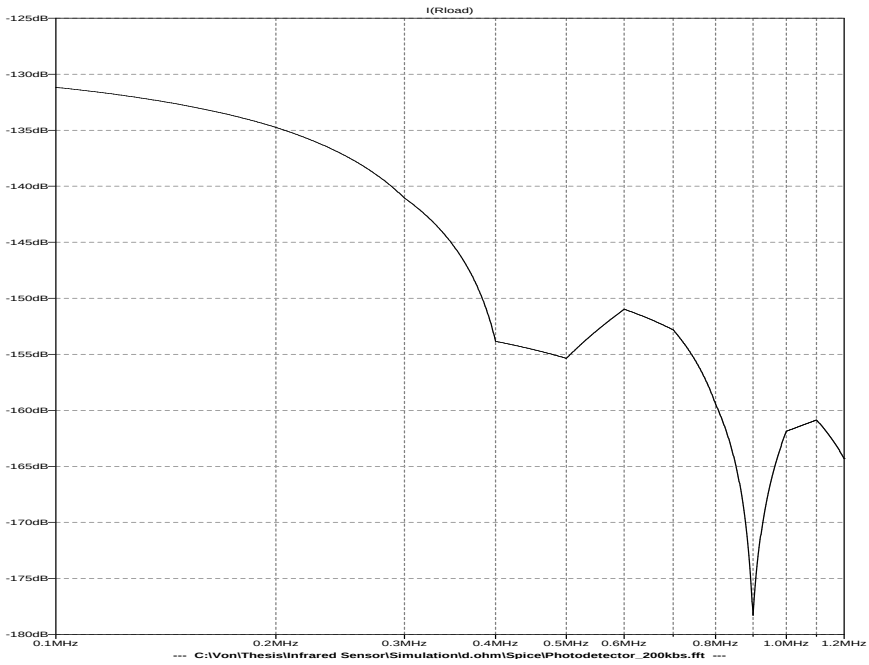

FIGURE 4.8: Photodiode Circuit Frequency Response

4.3. Experimental Results

4.3.1. RF Channel Measurements

The channel characteristics of the enclosure presented in Figure 4.9 were tested. The measurements obtained were the path loss and RMS delay spread. It is known that with these measurements a wireless channel can be fully characterized and understood [33][32]. An Agilent 8719ES S-parameter Vector Network Analyzer was used to perform this testing over the frequency range of 2.4GHz to 2.5GHz. The network analyzer was setup to take 1601 S_{21} measurements over the range specified.

This testing was performed under four different configurations: LOS box closed, LOS box open, NLOS box closed, and NLOS box open. A metal obstruction was placed in the LOS path to simulate the NLOS case and the open box consisted of one side being removed.

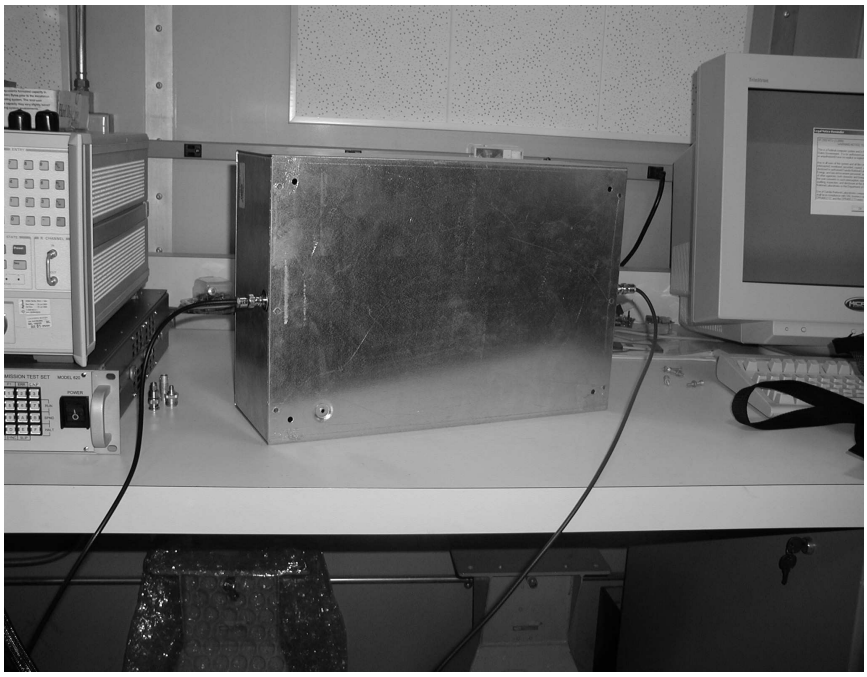

FIGURE 4.9: Test RF Enclosure

The results for each sweep were plotted in frequency versus S_{21} measured in dB and are presented in Figures 4.10, 4.11, 4.12, and 4.13 for each test configuration. These plots represent the frequency response of the channel and can be converted to the impulse response by Fourier analysis methods. After the 512-point inverse discrete Fourier transform has been performed, statistical processing can take place to determine the average path delay seen by a signal under each condition. The impulse response results are presented in Figures 4.14, 4.15, 4.16, and 4.17.

The time dispersive properties of wide band multipath channels are most commonly quantified by their mean excess delay ($\bar{\tau}$) and rms delay spread (σ_τ) which can be determined from the channel impulse response [26]. The mean excess delay is the first moment of the impulse response and is given by Equation (4.3) [26]

$$\bar{\tau} = \frac{\sum_k P(\tau_k)\tau_k}{\sum_k P(\tau_k)}. \tag{4.3}$$

The rms delay spread is the square root of the second central moment of the impulse

response and is given by 4.4.

$$\sigma_\tau = \sqrt{\bar{\tau^2} - \bar{\tau}^2} \tag{4.4}$$

where

$$\bar{\tau^2} = \frac{\sum_k P(\tau_k)\tau_k^2}{\sum_k P(\tau_k)}. \tag{4.5}$$

Table 4.3 presents results of the rms delay spread and mean excess delay for an enclosed box and a partially enclosed box under LOS and NLOS conditions. From these results and using the rule of thumb that the rms delay spread of the channel should not be greater than 10% of your symbol duration, it has been determined that the maximum symbol rate of this metal enclosure is 3 Msps.

Configuration	RMS Delay Spread	Mean Excess Delay	Units
LOS Closed	34	32	ns
LOS Open	8	7	ns
NLOS Closed	48	73	ns
NLOS Open	10	14	ns

TABLE 4.2: RMS Delay Spread for different LOS and NLOS situations

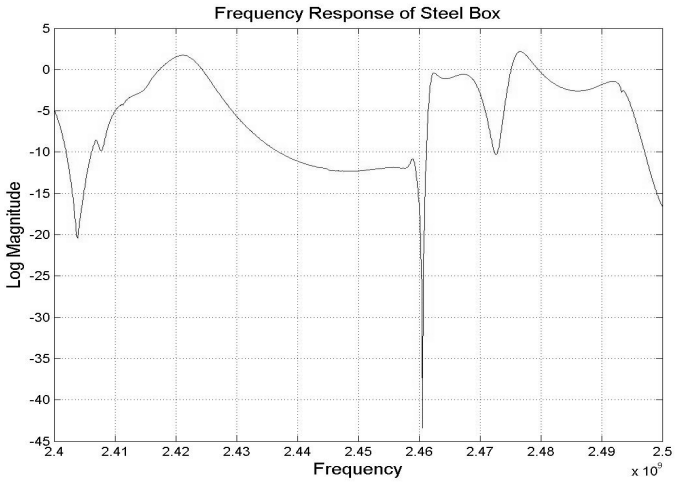

FIGURE 4.10: Frequency Response for the LOS Closed Box

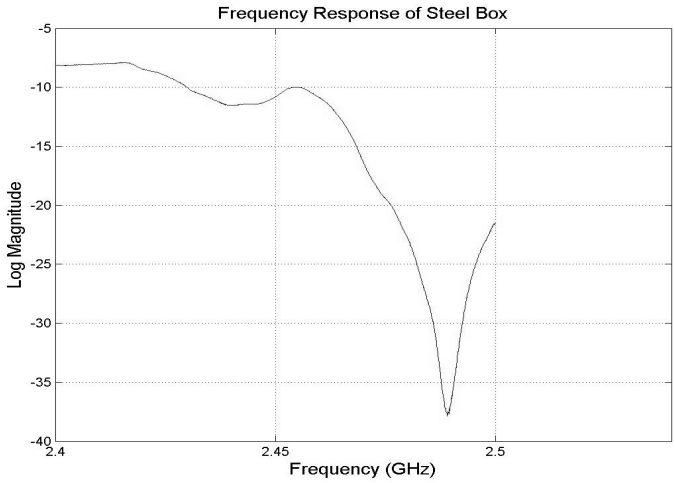

FIGURE 4.11: Frequency Response for the LOS Open Box

4.3.2. Optical Response of Different Materials

Table 4.3 presents the peak-to-peak voltage generated in the receiver and the optical power incident on the receiver. The transmitter had an average transmit current of 50mA, which corresponds to a transmit power of 15mW. The transmitter was turned on and off at a rate of 10KHz by a square wave. The different material responses can be compared to the line-of-sight air situation to establish a reference. The dull side of

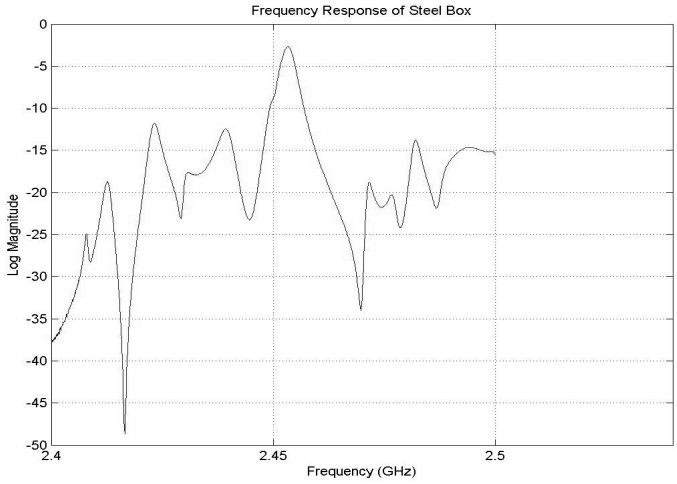

FIGURE 4.12: Frequency Response for the NLOS Closed Box

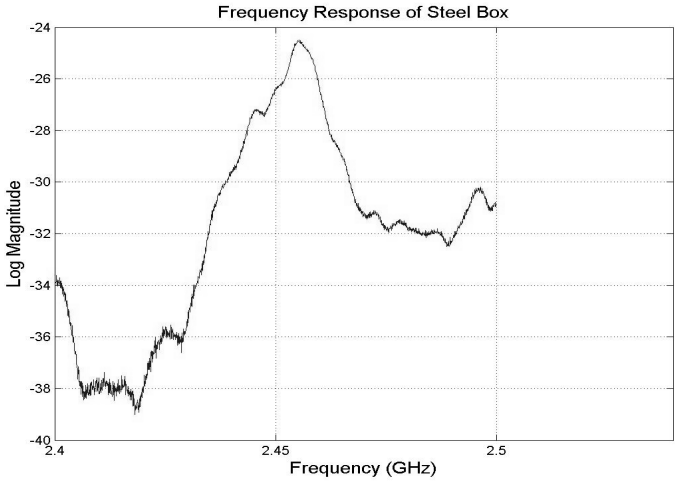

FIGURE 4.13: Frequency Response for the NLOS Open Box

aluminium foil and white paper have the best reflectivity. Tin and the shiny side of aluminium foil are very reflective in a specular sense, but that will not help when diffuse reflections are needed. A good diffuse reflector sends light in many directions and allows for a more even distribution of light. This even distribution increases the probability of light reaching the photodiode receiver.

The NLOS test setup consisted of the transmitter and receiver being $+45^o$ and -45^o from the normal to the surface they were testing. If a radial were drawn from the

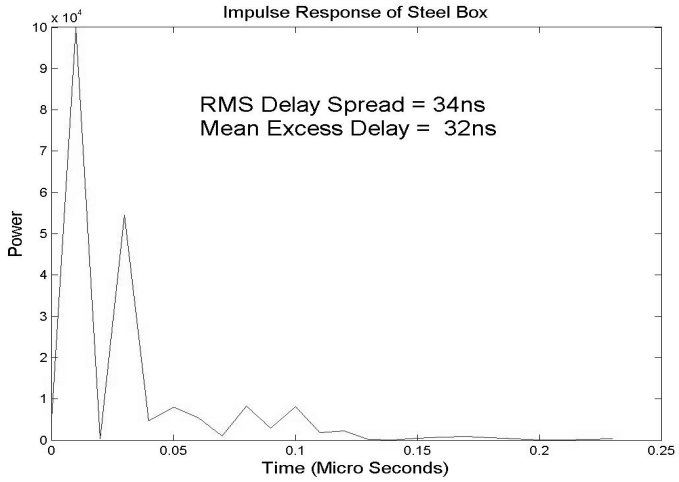

FIGURE 4.14: Impulse Response for the LOS Closed Box

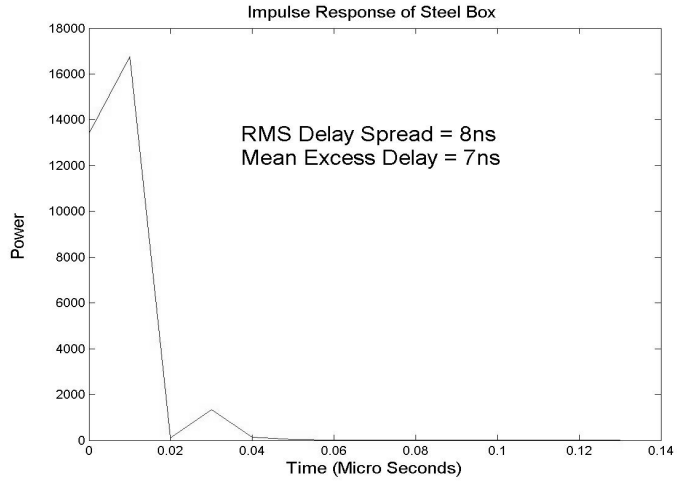

FIGURE 4.15: Impulse Response for the LOS Open Box

transmitter and receiver to the test surface, the angle formed by those two radials would be 90^o and the length of each radial would be 9 inches. In the LOS case (transmitter and receiver pointed at each other) there would be no test surface and the distance between transmitter and receiver would be 18 inches. The overall distance in all tests (LOS and NLOS) was 18 inches and a $100mm^2$ silicon photodiode (see Table 3.3) was used in the receiver. The peak-to-peak voltage was measured at the output of the receiver, which comes after the current amplifier. The optical power was measured using a Newport

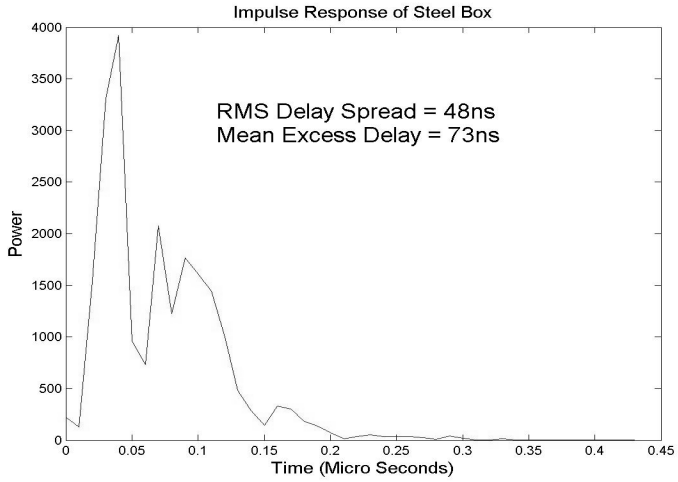

FIGURE 4.16: Impulse Response for the NLOS Closed Box

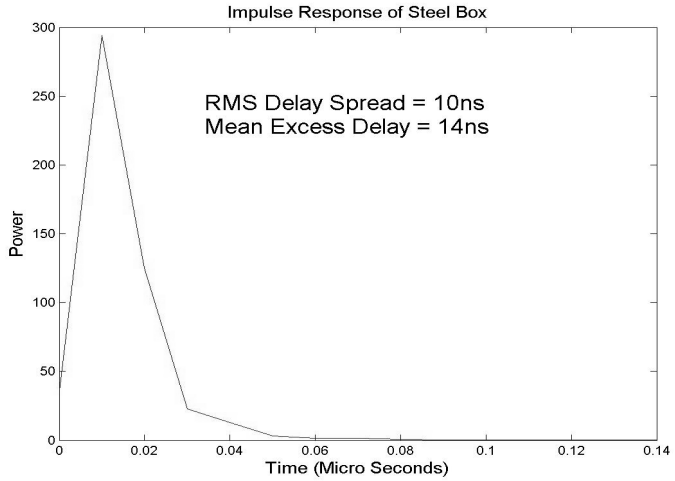

FIGURE 4.17: Impulse Response for the NLOS Open Box

Digital Power Meter (Model 815) with a Silicon Newport Photodetector (Model 818-SL).

Some unexpected results were encountered during this test, the black velvet should of yielded the worst performance and the Shiny aluminium should reflected better. The poor performance of shiny aluminium may be attributed to the transmitter and receiver being misaligned. Shiny aluminium will only reflect specularly and would require good alignment. The results are presented in Table 4.3.

Material	Peak to Peak Voltage (V)	Optical Power (uW)	Average "Reflection" Coefficient ρ
LOS	5.00	3.78	1.00
Aluminium Foil (DullSide)	4.40	3.45	0.90
White Paper	4.24	2.63	0.77
Black Velvet	3.80	2.21	0.67
Tin	3.52	2.26	0.65
Aluminium Foil (Shiny Side)	2.72	1.93	0.53

TABLE 4.3: Optical Response of Different Materials ($100mm^2$ PD)

4.3.3. Bit Error Rate Performance

The prototype system was primarily designed to operate and be tested at 100Kbps, but it could operate at transmission rates of 50Kbps up to 400Kbps. The transmitter sends RZ and NRZ OOK pulses using intensity modulation and the receiver employs direct detection. The system was tested in a large optical laboratory with no ambient light unless otherwise stated.

Power vs. BER

From Figures 4.18 and 4.19 it is clear that as the power is increased the performance improves to a point and then rapidly diminishes. This second performance degradation is what is known as receiver saturation. A way this is manifested is by over charging the photodiode capacitance. The load resistor is very large which leads to a large RC time constant and a long photodiode capacitance discharge time. If the photodiode is charged to a sufficient level and then slowly discharges, the current symbol may corrupt the next symbol, causing inter-symbol-interference.

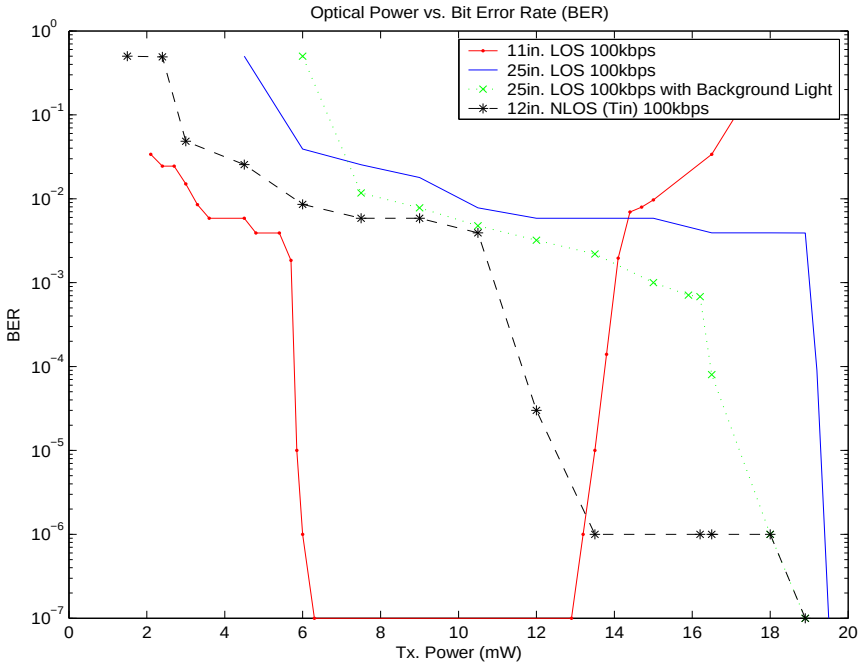

FIGURE 4.18: Optical Power in Milliwatts Versus Bit Error Rate

Data Rate vs. BER

In Figure 4.21, data rate versus BER was tested at two different temperatures. It can be seen that at a higher temperature the performance is worse. This is due to the transmit power being lower at higher temperatures for an LED. When the LED is on for long periods of time it will heat up. In this sensor application, the temperature issue can be mitigated by transmitting only periodically, e.g. once per second, which is acceptable for low-data-rate applications. When the LED is not transmitting, it will cool back to ambient temperature.

Distance vs. BER

In some situations, such as the one presented in Figure 4.22, a low power level background light helps to improve the performance. This additional ambient light increases the off-state bias level, causing the transmitter to be sightly on even when the

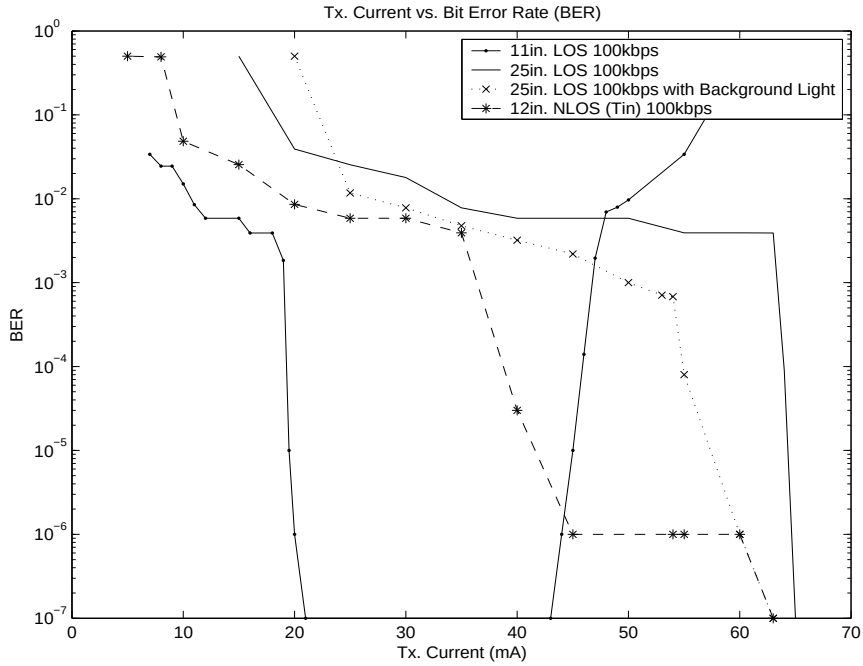

FIGURE 4.19: Transmitter Current in Milliamps Versus Bit Error Rate ($A_{PD} = 100mm^2$)

transmitter is in an off state. This can be attributed to the receiver circuit having sub-optimal performance.

Angular Diversity

Angular diversity was tested in the following four configurations: 1 transmitter and 1 receiver (SISO), 2 transmitters and 1 receiver(MISO), 1 transmitter and 2 receivers (SIMO), and 2 transmitters and 2 receivers (MIMO). These tests were conducted in a $24 \times 24 \times 26$ inch^3 tin box with an obstruction blocking 50% of the area between the transmitter and receiver. The results of these tests are shown in Figure 4.23.

Return-to-Zero Line Coding Performance

The return-to-zero (RZ) line coding was implemented in an effort to reduce transmit power and eliminate ISI. The schematic for converting from NRZ to RZ is presented

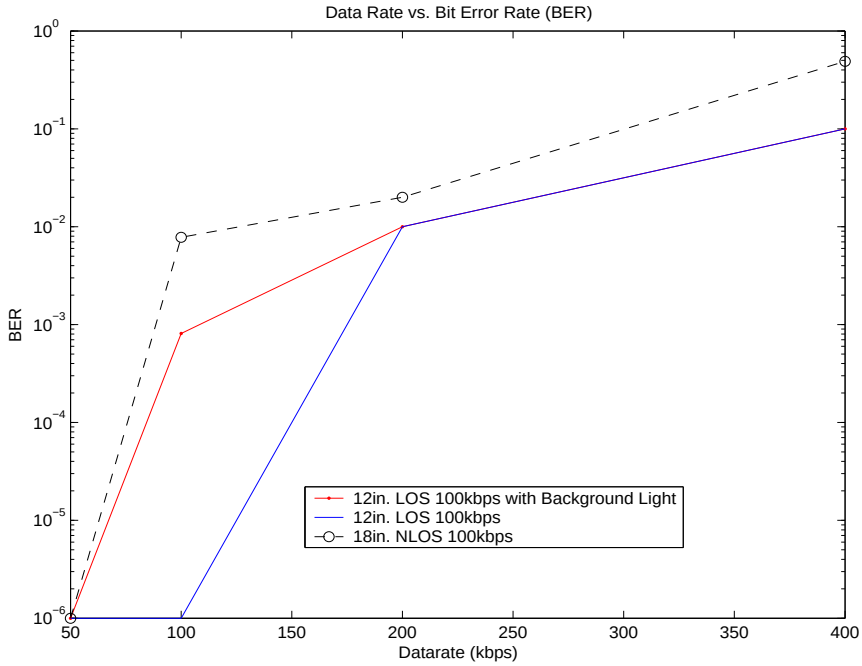

FIGURE 4.20: Datarate in Kbps Versus Bit Error Rate ($A_{PD} = 100mm^2$)

in Figure 4.24 and the results of this test are presented in Figure 4.25.

4.3.4. General Experimental Comments and Observations

Background Light

The presence of background light appears to improve the transmitter/receiver performance. At a distance of 20 inches, a transmit current of 50mA, and ambient light near the receiver of $0.5uW$, the BER can be improved from 10^{-3} to 10^{-6}. This could be due to the ambient light level being sufficient to partially turn on the photodetector while the transmitter is in the off state. When the transmitter does turn on, the photodetector does not have to come out of a cold state and can respond more quickly. An ambient light level of $0.5uW$ near the receiver is sufficient to take advantage of this phenomenon. Anything more that $1uW$ will begin to cause more errors. The ambient background

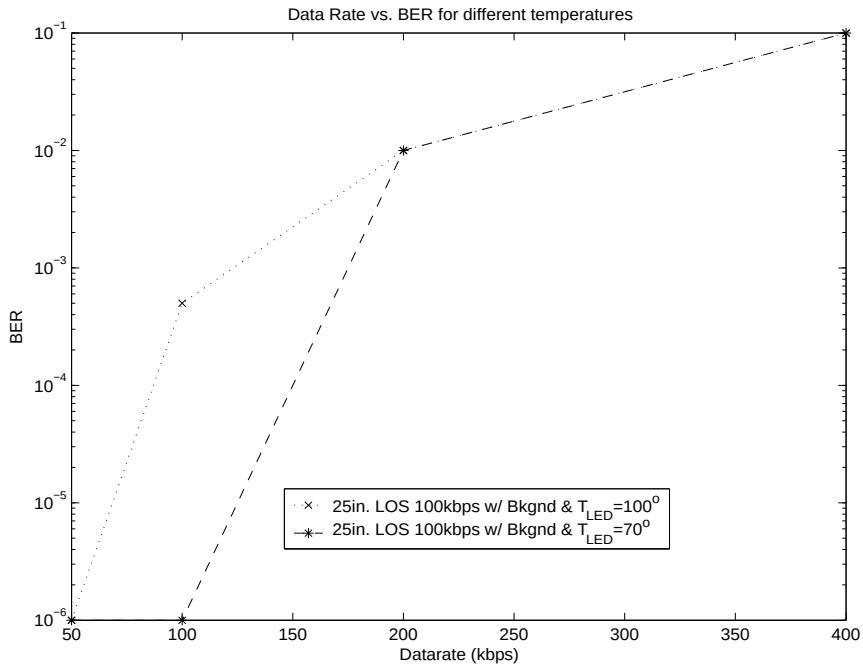

FIGURE 4.21: Datarate in Kbps Versus Bit Error Rrate at Two Different Temperatures

light level was measured with a Newport Digital Power Meter (Model 815) with a Silicon Newport Photodetector (Model 818-SL).

Measured Optical Power from Transmitter

The optical power at a distance of 20 inches was found to be $3.0uW$. The power was measured using the Newport Power Meter. The transmitter was set to an optical transmit power of 15mW or a current of 50mA.

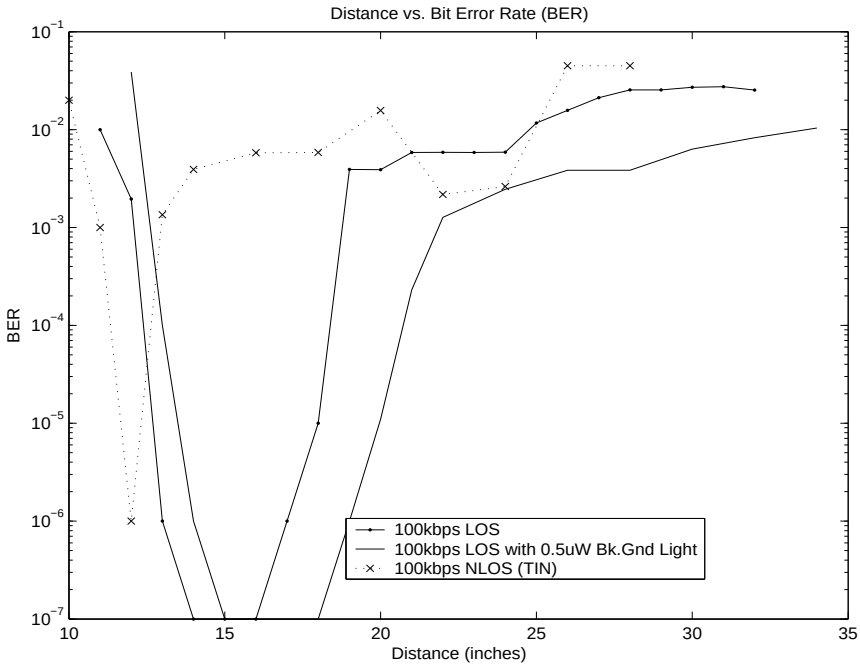

FIGURE 4.22: Distance Versus Bit Error Rate ($A_{PD} = 100mm^2$)

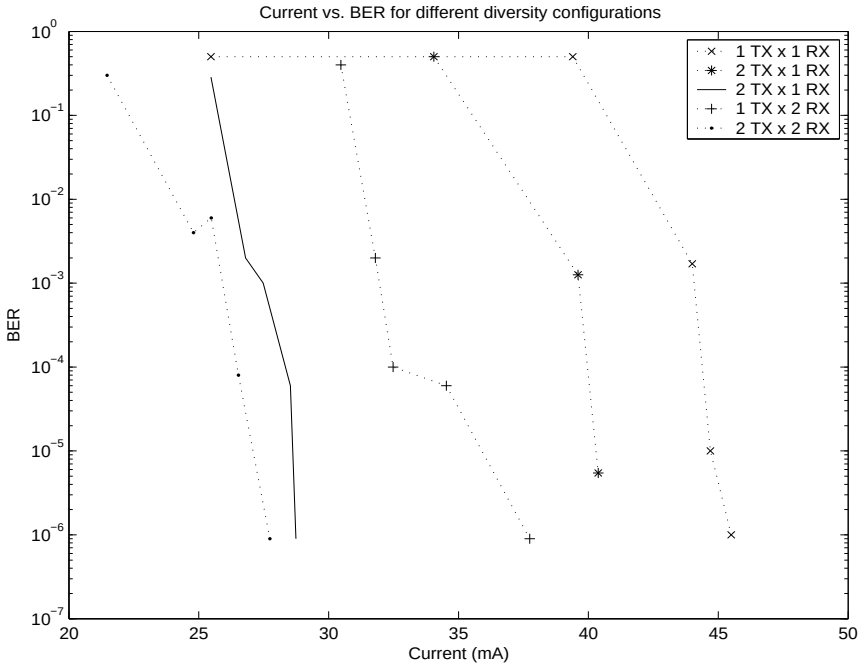

FIGURE 4.23: Transmitter Current Versus BER for Different Diversity Schemes ($A_{PD} = 35mm^2$)

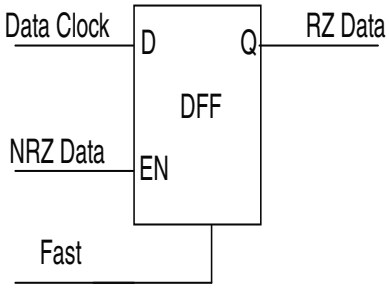

FIGURE 4.24: Return-to-Zero Encoder

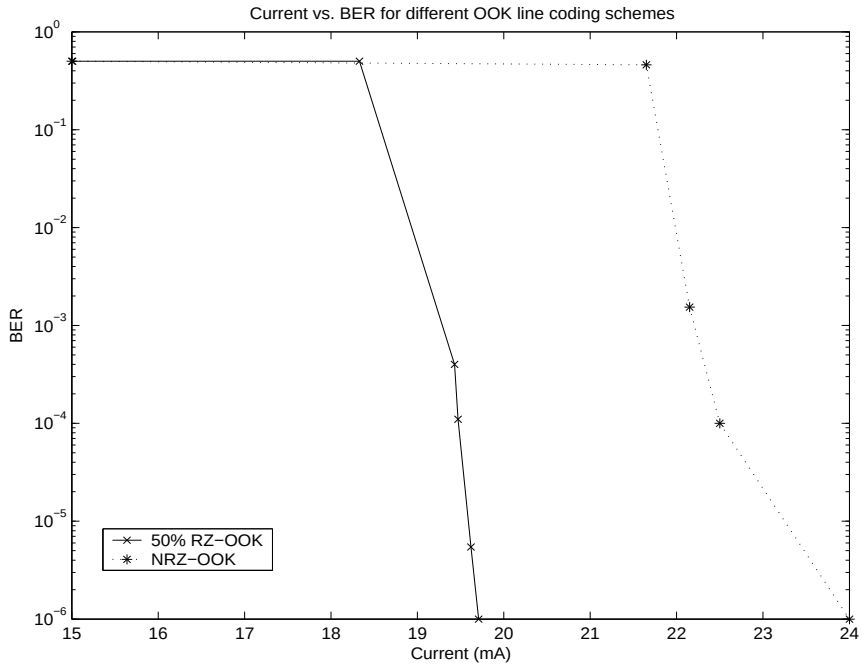

FIGURE 4.25: Transmitter Current versus BER for Different Line-Coding Schemes ($A_{PD} = 35mm^2$)

CHAPTER 5. CONCLUSION

This thesis deals with the design of a wireless optical sensor system for metal enclosed environments. Such a system could be used to eliminate wires that are otherwise necessary. The elimination of wires allows for rapid installation, easy reconfigurability, significant weight reduction, and thermal isolation. It is meant as a designer's guide, as it provides design rules and discusses many fundamental and practical limitations encountered in IR and RF system design. The emphasis is on low-power and low-complexity transmission, since the majority of the applications are battery operated.

Good understanding of the propagation channel and infrared system components was necessary. Using analytical techniques, simulation, and experimental measurements, the characterization of this infrared channel has been performed.

5.1. Summary of Results

1. Diffuse infrared light transmission with intensity modulation and direct detection (IM/DD) seems to be the best candidate for low-speed wireless communication for the target metal-enclosed environment.

2. The rms delay spread is not significant when compared to symbol duration, and thus should not cause ISI and limit system performance at low data rates.

3. Angular diversity can be used to improve the performance in short range diffuse optical communication environments. Diversity schemes, such as spatial, angular, frequency/wavelength, temporal, or polar diversity, can be implemented to improve performance. Due to the optical wavelength being many orders of magnitude smaller than a typical photodiode, the receiver has spatial diversity built in. Therefore, fading does not need to be accounted for. It has been shown that angular diversity is the best diversity

scheme for non-directed wireless infrared communication [7]. The benefit to angular diversity may be manifested in the following ways: reduced delay spread, increased SNR, increased power margin, and increased range. Multiple transmit beams and multiple photodetectors with a narrow FOV can improve the performance of non-directed wireless IR links. This performance improvement is due to the reduction of ambient noise and multipath distortion [7].

4. Decreasing the pulse duration increases power efficiency and mitigates inter-symbol-interference. Therefore, the best modulation scheme is RZ-OOK, which also offers the benefit of lower power in the transmitter and lower complexity in the receiver.

5. Better propagation with the lowest path loss could be achieved by carefully designing the interior surface of the metal enclosure. When considering NLOS communication a good diffuse surface must be employed, such as dull aluminum or white paint.

6. As the temperature of the LED increases, the optical transmit power decreases for a given current. This drop in power affects the bit error rate at the receiver. For example a change in temperature from 70 to 100 degrees Fahrenheit corresponds to a 12% decrease in transmit power and a hundred fold increase in BER (10^{-6} *to* 10^{-4}).

5.2. Summary of Contributions

1. Demonstrated the use of diffuse NLOS optical communication with diversity for metal-enclosed environments. System performance was provided through test results.

2. It has been shown for the first time that non-traditional diffuse communication within a small reflective enclosure is feasible.

3. Each part of the communication system has an impact on the achievable data rate: receiver, channel, and transmitter. The leading hindrance to higher data rates for NLOS diffuse communication is the capacitance experienced in the receivers's photodiode. This is due to the requirement of a large PD for diffuse NLOS communication.

Multipath delay in the channel causes ISI, which will eventually limit the data rate to below a few megahertz, although it may be combated with equalization. The third area of bandwidth limitation is in the transmitter LED. There are a couple tradeoffs that will be encountered when designing in an LED: response time for power efficiency and beamwidth for signal irradiance. Faster LED rise-times have lower electrical current to optical power efficiency. A summary of these results is presented in Table 5.1.

Optical Area	Impediment	Bandwidth
Receiver	Photodiode Capacitance	$\leq 200KHz$
Channel	Multipath ISI	$\leq 3MHz$
Transmitter	LED Response Time ($0.5us$)	$\leq 100KHz$

TABLE 5.1: Bandwidth Limitations For the System Designed

4. The temperature effect in the LED will have a drastic affect on the bit-error-rate performance if the transmitter is operated on a continuous basis.

5.3. Future Research

The Future Research subsection is included so that researchers picking up this work in the future have the benefit of the ideas that were generated during this thesis.

5.3.1. Advanced Topics

In this section we will discuss some more advanced options that could be used to improve the performance.

Positioning

The effect of shadowing, tilt or receiver location greatly affects the overall transmitted signal propagation and can only be determined experimentally [27]. The optical design in the presence of additional impediments, such as receiver tilt, shadowing, multipath dispersion, and electronic receiver noise, should be explored. Diversity can be used to improve the chances of achieving a good position.

Diversity Techniques

Using a more optimal combining technique should improve the performance even further beyond the simple selection combining method. Using multiple photodiodes in the receiver with a smaller area and hence a smaller capacitance could greatly increase the bandwidth. The receiver FOV would be the same, except split-up into sections. If selection diversity is used with this scheme the capacitance encountered at the receiver would be from one of the smaller photodiodes.

Power Efficient Modulation

A low-power low-complexity PPM test setup was presented in Chapter 2. Unfortunately this setup was not tested. Future research could be focused on developing a prototype for this modulation scheme.

Clock Recovery

An accurate clock recovery scheme is imperative to good BER performance. Therefore, other areas to explore could include a better clock recovery scheme in the receiver, such as using a phase lock loop to extract the clock from demodulated data.

Front End Amplifier

Further investigation into the receiver front end amplifier options would be a worthy topic to investigate since the primary source of receiver noise stems from this part of the system. Use of an avalanche photodiode in place of a standard PIN photodiode

could be incorporated into this study. Various amplifier options include: using a transistor (BJT or FET) or transimpedance amplifier (OP-AMP). Another area to investigate with receiver amplifier design is minimizing the photodiode capacitance by using bootstrapping techniques.

5.3.2. Digital Processing Algorithms for IR

The following sub-sections will discuss some baseband processing algorithms and their application to optical communication systems.

Spreading

This digital processing technique uses either a direct-sequence (DS) or a frequency-hopping method to spread information over a wide bandwidth [22]. This spread spectrum technique provides interference-immune communications in adverse optical interference conditions and in the presence of intentional or unintentional jamming . The direct sequence technique transforms information symbols into small segments called chips using a spreading code such as a Barker Code or a PN Code. DS will require having an LED and PD that can transmit and receive pulses of shorter duration, temporally speaking. In the transmitter this translates to a shorter rise time requirement and in the receiver, this means designing for a lower capacitance front-end.

If the location of other optical interferers is unknown, frequency hopping or wavelength hopping may be a beneficial technique to try. Each hopping wavelength should be 50 nm to 100 nm apart. The photodetector must be chosen such that it is sensitive to all the wavelengths transmitted. A separate LED would be required for each transmission wavelength.

Coding

Channel encoding of the source data results in an increased reliability and fidelity of the received data and signal. Coding techniques can be used for spectrum control

(e.g. by using different line codes) or error control purposes [22]. Error control coding (ECC) or channel coding converts a sequence of digitally modulated bits into a block or sequence of channel bits. These sequences are referred to as code words and can be decoded back to the source data, correcting errors along the way. There are many different error correction algorithms, but the ones that seem most appropriate for a low power wireless optical system are convolutional codes or linear codes. The justification for this is due to the low complexity and low power of these error correction algorithms. Anything more complicated such as iterative turbo decoding or soft decision significantly increases the power required or decoding complexity, respectively. It is noted that this only occurs in the receiver. Further research and testing with a good convolutional encoder with Viterbi decoding or a block code should be considered.

Pulse Shaping

If the channel characteristics are known, pre-filtering the information carrying pulse that will enter the channel has been shown to lower the signal distortion that is observed in the receiver [8]. Gaussian pulse shaping has been found to provide the best performance for infrared wireless communication [10].

Equalization

Equalization becomes necessary in communication systems where the data rate is greater than 10Mbps for diffuse and 100Mbps for LOS due to ISI [9]. For such systems a zero-forcing decision-feedback equalizer (ZF-DFE) is recommended if the channel characteristics are unknown and dynamic. If the channel properties are known and quasi-static a MSE equalizer will suffice.

A Appendices

A1. Abbreviations

Abbreviation	Definition
AD	Angle Diversity
ADC	Analog to Digital Converter
APD	Avalanche Photodiode
AWGN	Additive White Gaussian Noise
BER	Bit Error Rate
BJT	Bipolar Junction Transistor
BPF	Band Pass Filter
BW	Band Width
DD	Direct Detection
DPPM	Differential Pulse Position Modulation
DSSS	Direct Sequence Spread Spectrum
EG	Equal Gain
eV	Electron Volts
FET	Field Effect Transistor
FHSS	Frequency Hopping Spread Spectrum
FOV	Field of View
FPGA	Field Programmable Gate Array
FS	Frame Synchronization
GaAs	Gallium Arsenide
GHz	Gigahertz
HOE	Holographic Optical Element
HPM	Holographic Parabolic Mirror
HSM	Holographic Spherical Mirror
IM	Intensity Modulation
IR	Infrared

ISI	Inter-Symbol Interference
KHz	Kilohertz
LD	Laser Diode
LED	Light Emitting Diode
LFSR	Linear Feedback Shift Register
lm	Lumens
LOS	Line of Sight
LPF	Low Pass Filter
MHz	Megahertz
MLSD	Maximum Likelihood Sequence Detection
MMSE	Minimum Mean Square Error
MOSFET	Metal Oxide Semiconductor Field Effect Transistor
MSE	Mean Square Error
MR	Maximal Ratio
NEP	Noise Equivalent Power
NLOS	Non-Line of Sight
NRZ	Non-Return-Zero
OOK	On-Off Keying
PD	Photo Detector
PIN	Positive Intrinsic Negative
PLL	Phase Lock Loop
PN	Pseudo-Random Number
PPM	Pulse Position Modulation
PRBS	Pseudo Random Bit Stream
PS	Pulse Shape
QE	Quantum Efficiency
QoS	Quality of Service

QPSK	Quadrature Phase Shift Keying
RMS	Root Mean Square
RZ	Return-to-Zero
S&H	Sample and Hold
SB	Select Best
SC	Semi-Conductor
Si	Silicon
SNR	Signal-to-Noise Ratio
SS	Slot Synchronization
T&H	Track and Hold
THz	Terahertz
TPC	Turbo Product Code
ZF-DFE	Zero Forcing Decision Feedback Equalizer

A2. Prototype Bill of Material (BOM)

Qty.	Item	Manufacturer	Part Number
2	LED	Opto-Diode	OD-880E
2	$35mm^2$ Silicon Photodiode	Centrovision	OSD35-3T
1	$100mm^2$ Silicon Photodiode	Centrovision	OSD100-0A
2	FPGA Prototype Board	Parallax / Altera	Cyclone Fastpack
2	NPN BJT Transistor	Motorolla	3904
1	Variable Resistor	Radioshack	1-Turn 50KΩ
2	Variable Resistor	Radioshack	15-Turn 1KΩ
4	Prototyping Boxes With PCB Board	Radioshack	RS10129
x	Various Through Hole Resistors	Philips	NA

A3. Prototype Pictures

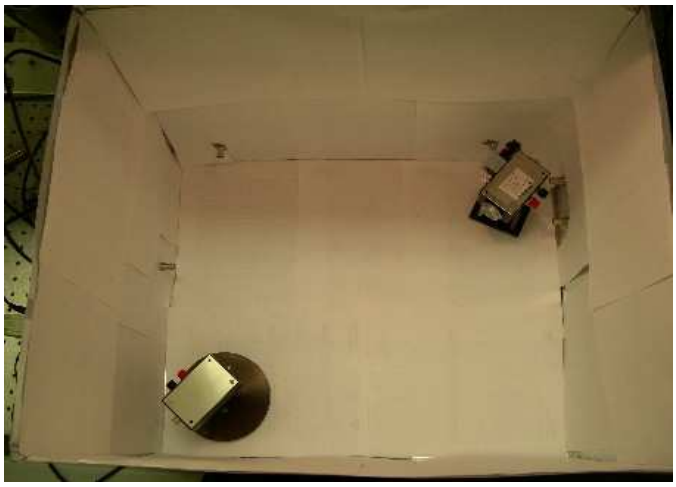

FIGURE 5.1: Inside of Metal Enclosure

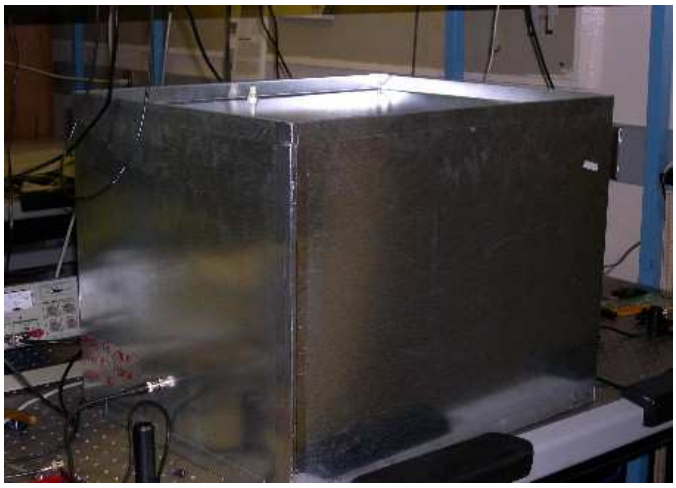

FIGURE 5.2: Outside of Metal Enclosure

FIGURE 5.3: Transmitter Front-End

FIGURE 5.4: Receiver Front-End with $35mm^2$ PD

FIGURE 5.5: Receiver Front-End with $100mm^2$ PD

A4. FPGA AHDL Source Code

100kbps NRZ-OOK

```
---------
-- TOP --
---------
include "pxl_.inc"; include "altpll.inc"; include
"altsyncram.inc"; subdesign top (
    jclk        : input;        -- clock socket input
\vspace{0.5 in}
    pclk        : input;        -- plugboard clock input
    rx          : input;        -- serial receive
    tx          : output;       -- serial transmit
    btn[2..0]   : input;        -- pushbutton inputs
    led[7..0]   : output;       -- led outputs
    spk[1..0]   : output;       -- speaker outputs
    h[31..0]    : bidir;        -- header pins, may be inputs, outputs, or bidirect
    p[11..1]    : bidir;        -- plugboard pins, may be inputs, outputs, or bidir
    p0          : input;        --
    px[2..0]    : input;        -- px loader pins, must be inputs
)
 variable
    pll         : altpll with ( -- pll
                    operation_mode = "normal",
                    inclk0_input_frequency = 20000,     -- inclk0 = 20,000ps = 50MH
                    clk0_multiply_by = 4,               -- clk0 = 50MHz*4/1 = 200MH
                    clk0_divide_by = 1,
                    clk1_multiply_by = 2,               -- clk1 = 50MHz*2/5 = 20MHz
```

```
                    clk1_divide_by = 5);
    clkfast     : node;         -- clocks
    clkslow     : node;
--  pn7sr[6..0] : dff;          -- Shift Register for PN7
generator
    pn9sr[8..0] : dff;          -- Shift Register for PN7 generator
    reset[5..0] : dffe;         --
    reset_pls   : dff;          --
    pclk_out    : dff;          --
    cnt[32..0]  : dff;          -- big counter
--  cntdelay[7..0]  : dffe ;    -- Delay Counter for DPLL --  TC :
node ;    -- Terminal Count
    htri[31..0] : tri;          -- tri's for plugboard and header pins
    ptri[11..1] : tri;          --
    ptri0       : node;         --
    tone[1..0]  : node;         -- tone pair
    pxl         : pxl_          -- pxl (512 x 8)
                  with (
                    a_exp = 9,
                    d_exp = 3);
    ram         : altsyncram    -- ram (512 x 8)
                  with (
                    operation_mode = "single_port",
                    widthad_a = 9,
                    width_a = 8);
    edgedet_sr[1..0]    : dff;          -- Shift register for finding data edge
    datarx      : node;         -- Data receive node
    edge        : node;         -- edge pulse
```

```
    dpllr[11..0]        : dff;          -- counter for clock recovery
    dpllr_div   : dff;          -- divide and delay clock
begin
    -- Reset Counter
    reset[].clk = cnt[12];
    reset[].ena = !reset5;
    reset[]     = reset[] + 1;
    reset_pls.clk = cnt[11];
    reset_pls = (reset== 0) OR (reset== 1) OR (reset== 2) OR (reset== 3) OR (reset=
    -- pll/clocks
    pll.inclk0          = jclk;                 -- connect jclk to pll input
    pll.clkena[]        = b"11";                -- enable both pll outputs
    clkfast             = pll.clk0;             -- assign 200MHz pll output to clkf
    clkslow             = pll.clk1;             -- assign 100kHz pll output to clks
    -- counter
    cnt[].clk           = clkfast;              -- count fast
    cnt[].d             = cnt[].q + 1;
    -- use pushbuttons to select tone
    case btn[] is
        when b"110"     => tone[] = (cnt[15], !cnt[15]);
        when b"101"     => tone[] = (cnt[16], !cnt[16]);
        when b"100"     => tone[] = (cnt[17], !cnt[17]);
        when b"011"     => tone[] = (cnt[18], !cnt[18]);
        when b"010"     => tone[] = (cnt[19], !cnt[19]);
        when b"001"     => tone[] = (cnt[20], !cnt[20]);
        when b"000"     => tone[] = (cnt[21], !cnt[21]);
        when others     => tone[] = gnd;
    end case;
```

```
    spk[]               = tone[] & cnt[24].q & cnt[25].q;
    -- echo rx to tx
    tx                  = rx;
    -- PX Loader example
    pxl.clk             = clkfast;
    pxl.px[]            = px[];
    ram.clock0          = clkfast;
    case pxl.load is
        when 0          => ram.wren_a       = gnd;
                           ram.address_a[]  = cnt[24+8..24+0].q;
                           ram.data_a[]     = gnd;
        when 1          => ram.wren_a       = pxl.w;
                           ram.address_a[]  = pxl.a[];
                           ram.data_a[]     = pxl.d[];
    end case;
    -- output ram data to LEDs
    --led[] = ram.q_a[];
    led0      = btn[2] & btn[1] & btn[0];
    led1      = btn[2] & btn[1] & !btn[0];
    led2      = btn[2] & !btn[1] & btn[0];
    led3      = btn[2] & !btn[1] & !btn[0];
    led4      = !btn[2] & btn[1] & btn[0];
    led5      = !btn[2] & btn[1] & !btn[0];
    led6      = !btn[2] & !btn[1] & btn[0];
    led7      = !btn[2] & !btn[1] & !btn[0];
-- PN7 Generator (LFSR PRBS) --  pn7sr[6..0].clk = cnt[10]; --  IF
reset_pls THEN --      pn7sr[6..0] = B"1111111"; --  ELSE --
pn7sr[6..1] = pn7sr[5..0]; --      pn7sr[0] = pn7sr[5] XOR
```

```
pn7sr[6]; --  END IF; -- PN9 Generator (LFSR PRBS)
    pn9sr[8..0].clk = cnt[10];
    IF reset_pls THEN
        pn9sr[8..0] = B"111111111";
    ELSE
        pn9sr[8..1] = pn9sr[7..0];
        pn9sr[0] = pn9sr[4] XOR pn9sr[8];
    END IF;
-- Reset DPLL counter less often --  cntdelay[].clk          =
clkslow; --cnt[10];           -- count fast --  cntdelay[].ena =
edge; --  cntdelay[].clrn         = vcc;              -- --
cntdelay[].d            = cntdelay[].q + 1; -- --  IF cntdelay ==
B"11111111" THEN --      TC = vcc; --  ELSE --      TC = gnd; --
END IF; -- DPLL, Receiver Clock Recovery
    edgedet_sr[1..0].clk = clkslow;             -- Shift Register to detect bit edg
    edgedet_sr[1] = edgedet_sr[0];
    edgedet_sr[0] = datarx;
    edge = !edgedet_sr0 and edgedet_sr1;        -- Bit edge occurs
    dpllr[11..0].clk = clkfast;                 -- Counter to maintain repeating cl
    dpllr[11..0].clrn = !edge; --!TC;               -- Reset counter when edge is c
    dpllr = dpllr + 1;
    dpllr_div.clk = !dpllr[11];
    dpllr_div = !dpllr_div;
    pclk_out.clk = clkfast;
    pclk_out = pclk;
    -- output counter to IO pins
    htri[].oe           = vcc;
    htri[]              = cnt[31..0];
```

```
    h[]                 = htri[];
    ptri[].oe           = vcc;
    ptri[]              = (pn9sr[8], !cnt[10], cnt[10..7], dpllr[10], datarx, reset
    p[]                 = ptri[];
    ptri0               = p0;
    datarx              = ptri0;
end;
```

100kbps NRZ-OOK

```
---------
-- TOP --
---------
include "pxl_.inc"; include "altpll.inc"; include
"altsyncram.inc"; subdesign top (
    jclk        : input;        -- clock socket input
    pclk        : input;        -- plugboard clock input
    rx          : input;        -- serial receive
    tx          : output;       -- serial transmit
    btn[2..0]   : input;        -- pushbutton inputs
    led[7..0]   : output;       -- led outputs
    spk[1..0]   : output;       -- speaker outputs
    h[31..0]    : bidir;        -- header pins, may be inputs, outputs, or bidirect
    p[11..1]    : bidir;        -- plugboard pins, may be inputs, outputs, or bidir
    p0          : input;        --
    px[2..0]    : input;        -- px loader pins, must be inputs )
variable
    pll         : altpll with ( -- pll
                    operation_mode = "normal",
```

```
                    inclk0_input_frequency = 20000,     -- inclk0 = 20,000ps = 50MH
                    clk0_multiply_by = 4,               -- clk0 = 50MHz*4/1 = 200MH
                    clk0_divide_by = 1,
                    clk1_multiply_by = 2,               -- clk1 = 50MHz*2/5 = 20MHz
                    clk1_divide_by = 5);
    clkfast     : node;         -- clocks
    clkslow     : node;
--  pn7sr[6..0] : dff;          -- Shift Register for PN7
generator
    pn9sr[8..0] : dff;          -- Shift Register for PN7 generator
    reset[5..0] : dffe;         --
    reset_pls   : dff;          --
    pclk_out    : dff;          --
    cnt[32..0]  : dff;          -- big counter
--  cntdelay[7..0]  : dffe ;    -- Delay Counter for DPLL --  TC :
node ;    -- Terminal Count
    htri[31..0] : tri;          -- tri's for plugboard and header pins
    ptri[11..1] : tri;          --
    ptri0       : node;         --
    tone[1..0]  : node;         -- tone pair
    pxl         : pxl_          -- pxl (512 x 8)
                  with (
                    a_exp = 9,
                    d_exp = 3);
    ram         : altsyncram    -- ram (512 x 8)
                  with (
                    operation_mode = "single_port",
                    widthad_a = 9,
```

```
                    width_a = 8);
    data50duty  : dffe;     -- 50% duty cycle encoder
    edgedet_sr[1..0]    : dff;          -- Shift register for finding data edge
    datarx      : node;         -- Data receive node
    edge        : node;         -- edge pulse
    dpllr[11..0]        : dff;          -- counter for clock recovery
    dpllr_div   : dff;          -- divide and delay clock
begin
    -- Reset Counter
    reset[].clk = cnt[12];
    reset[].ena = !reset5;
    reset[]     = reset[] + 1;
    reset_pls.clk = cnt[11];
    reset_pls = (reset== 0) OR (reset== 1) OR (reset== 2) OR (reset== 3) OR (reset=
    -- pll/clocks
    pll.inclk0          = jclk;                 -- connect jclk to pll input
    pll.clkena[]        = b"11";                -- enable both pll outputs
    clkfast             = pll.clk0;             -- assign 200MHz pll output to clkf
    clkslow             = pll.clk1;             -- assign 100kHz pll output to clks
    -- counter
    cnt[].clk           = clkfast;              -- count fast
    cnt[].d             = cnt[].q + 1;
    -- use pushbuttons to select tone
    case btn[] is
        when b"110"     => tone[] = (cnt[15], !cnt[15]);
        when b"101"     => tone[] = (cnt[16], !cnt[16]);
        when b"100"     => tone[] = (cnt[17], !cnt[17]);
        when b"011"     => tone[] = (cnt[18], !cnt[18]);
```

```
    when b"010"     => tone[] = (cnt[19], !cnt[19]);
    when b"001"     => tone[] = (cnt[20], !cnt[20]);
    when b"000"     => tone[] = (cnt[21], !cnt[21]);
    when others     => tone[] = gnd;
end case;
spk[]               = tone[] & cnt[24].q & cnt[25].q;
-- echo rx to tx
tx                  = rx;
-- PX Loader example
pxl.clk             = clkfast;
pxl.px[]            = px[];
ram.clock0          = clkfast;
case pxl.load is
    when 0          => ram.wren_a       = gnd;
                       ram.address_a[]  = cnt[24+8..24+0].q;
                       ram.data_a[]     = gnd;
    when 1          => ram.wren_a       = pxl.w;
                       ram.address_a[]  = pxl.a[];
                       ram.data_a[]     = pxl.d[];
end case;
-- output ram data to LEDs
--led[] = ram.q_a[];
led0      = btn[2] & btn[1] & btn[0];
led1      = btn[2] & btn[1] & !btn[0];
led2      = btn[2] & !btn[1] & btn[0];
led3      = btn[2] & !btn[1] & !btn[0];
led4      = !btn[2] & btn[1] & btn[0];
led5      = !btn[2] & btn[1] & !btn[0];
```

```
    led6      = !btn[2] & !btn[1] & btn[0];
    led7      = !btn[2] & !btn[1] & !btn[0];
-- PN7 Generator (LFSR PRBS) --  pn7sr[6..0].clk = cnt[10]; --  IF
reset_pls THEN --      pn7sr[6..0] = B"1111111"; --  ELSE --
pn7sr[6..1] = pn7sr[5..0]; --      pn7sr[0] = pn7sr[5] XOR
pn7sr[6]; --  END IF; -- PN9 Generator (LFSR PRBS)
    pn9sr[8..0].clk = cnt[10];
    IF reset_pls THEN
        pn9sr[8..0] = B"111111111";
    ELSE
        pn9sr[8..1] = pn9sr[7..0];
        pn9sr[0] = pn9sr[4] XOR pn9sr[8];
    END IF;
-- RZ Shift Register --  data50duty.clk = cnt[9]; --  IF reset_pls
THEN --      data50duty[1..0] = B"00"; --  ELSE IF pn9sr[8] THEN
--      data50duty[1] = data50duty[0]; --      data50duty[0] = 1;
--  ELSE --      data50duty[1] = data50duty[0]; -- data50duty[0] =
0; --  END IF; -- RZ Mux --  IF cnt[9] THEN --      data50duty =
cnt[10]; -- ELSE --      data50duty = 0; --  END IF; -- NRZ to RZ
conversion data50duty.clk = clkslow;       -- over clocked
flip-flop data50duty.ena = pn9sr[8];  --cnt[11];  -- data control
data50duty = cnt[10]; -- Reset DPLL counter less often --
cntdelay[].clk = clkslow; --cnt[10];           -- count fast --
cntdelay[].ena = edge; --  cntdelay[].clrn         = vcc; -- --
cntdelay[].d = cntdelay[].q + 1; -- --  IF cntdelay == B"11111111"
THEN -- TC = vcc; --  ELSE --      TC = gnd; -- END IF; -- DPLL,
Receiver Clock Recovery
    edgedet_sr[1..0].clk = clkslow;             -- Shift Register to detect bit edg
```

```
    edgedet_sr[1] = edgedet_sr[0];
    edgedet_sr[0] = datarx;
    edge = !edgedet_sr0 and edgedet_sr1;        -- Bit edge occurs
    dpllr[11..0].clk = clkfast;                 -- Counter to maintain repeating cl
    dpllr[11..0].clrn = !edge; --!TC;               -- Reset counter when edge is c
    dpllr = dpllr + 1;
    dpllr_div.clk = !dpllr[11];
    dpllr_div = !dpllr_div;
    pclk_out.clk = clkfast;
    pclk_out = pclk;
    -- output counter to IO pins
    htri[].oe           = vcc;
    htri[]              = cnt[31..0];
    h[]                 = htri[];
    ptri[].oe           = vcc;
    ptri[]              = (pn9sr[8], !cnt[10], data50duty, cnt[10..8], dpllr[10], c
    p[]                 = ptri[];
    ptri0               = p0;
    datarx              = ptri0;
end;
```

BIBLIOGRAPHY

1. J. M. Kahn and J. R. Barry, "Wireless Infrared Communications," *Proceedings of the IEEE*, vol. 85, no. 2, pp. 265-98. Feb. 1997.

2. J. B. Carruthers, "Wireless Infrared Communications," *Wiley Encylopedia of Telecommunications*, pp. 1-7, 2002(Preprint).

3. J. B. Carruthers and J. M. Kahn, "Modeling of Non-Directed Wireless Infrared Channels," *IEEE Transactions on Communications*, pp. 1260-1268, Oct. 1997.

4. M. Kavehrad and S. Jikova, "Indoor Broadband Optical Wireless Communication: Optical Subsystems Designs and Their Impact on Channel Characteristics," *IEEE Wireless Communications*, vol.10, no.2, pp. 30-35, April 2003.

5. J. R. Barry, J. M. Kahn, W. J. Krause, E. A. Lee, and D. G. Messerschmitt "Simulation of Multipath Impulse Response for Indoor Wireless Optical Channels," *IEEE Journal on Selected Areas in Communications*, vol.11, no.3, pp. 367-379, Apr. 1993.

6. D. Shiu, and J. M. Kahn, "Differential Pulse-Position Modulation for Power-Efficient Optical Communication," *IEEE Transactions on Communications*, vol. 47, no. 8, pp. 1201-1208, Aug. 1999.

7. J. B. Carruthers and J. M. Kahn, "Angle Diversity for Nondirected Wireless Infrared Communication," *IEEE Transactions on Communications*, pp. 960-969, June 2000.

8. D. C. M. Lee, and J. M. Kahn, "Coding and Equalization for PPM on Wireless Infrared Channels," *IEEE Transactions on Communications*, vol. 47, no. 2, pp. 255-259, Feb. 1999.

9. K. K. Wong and T. O'Farrell, "Spread Spectrum Techniques for Indoor Wireless IR Communication," *IEEE Wireless Communications*, vol.10, no.2, pp. 54-63, April 2003.

10. A. Garcia-Zambrana, P. Vera-Candeas and A. Puerta-Notario, "Gaussian Pulse Shaping of Coded OOK Formats in Wireless Infrared Links at Hight Bit Rates," *IEEE Vehicular Technology Conference*, pp. 1094-1098, 2001.

11. http://www.irda.org/, June 2004.

12. http://grouper.ieee.org/groups/802/11/main.html/, June 2004.

13. J. R. Barry, "Wireless Infrared Communications," *Boston: Kluwer Academic Publishers*, 1994.

14. N. Moraitis, A. Kanatas, G. Pantos, P. Constantinou, "Delay Spread Measurements and Characterization in a Special Propagation Environment for PCS Microcells," *Proceedings of 13th IEEE International Symposium on Personal Indoor and Mobile Radio Communications*, Vol. 3, pp. 1190, 2002.

15. D. C. Cox and R. P. Leck, "Correlation Bandwidth and Delay Spread Multipath Propagation Statistics for Urban Mobile Radio Channels," *IEEE Transactions on Communications*, no. 11, Nov. 1975 pp.1271-1280

16. D. J. T. Heatley, D. R. Wisely, I. Neild and P. Cochrane, "Optical Wireless: The Story So Far" *IEEE Communications Magazine*, vol. 36, no.12, pp. 72-82, Dec. 1998.

17. R. Otte, L. P. de Jong, and A. H. M. van Roermund, "Low-Power Wireless Infrared Communications," *Boston: Kluwer Academic Publishers*, 1999.

18. J. C. Palais, "Fiber Optic Communications," *Pearson Education*, 4th Edition, 1998.

19. http://www.CentroVision.com/, June 2004.

20. S. B. Alexander, "Optical Communication Receiver Design," *Bellingham, WA, USA: SPIE Optical Engineering Press*, 1997.

21. http:// www.newwaveinstruments.com/, June 2004.

22. H. Liu, "ECE669 Lecture Notes," *Oregon State University: Electrical Engineering and Computer Science Department*, Fall 2003.

23. T. K. Plant, "ECE583 Lecture Notes," *Oregon State University: Electrical Engineering and Computer Science Department*, Spring 2004.

24. T. K. Plant, and D. Ohm, "ECE583 Lab Notes," *Oregon State University: Electrical Engineering and Computer Science Department*, Spring 2004.

25. http://www.optodiode.com/, Part Number OD-889E, June 2004.

26. T. S. Rappaport, *Wireless Communications – Principles and Practices*. Englewood Cliffs, NJ: Prentice-Hall, 2nd ed., 2002.

27. M. Wolf, and D. Kreb, "Short-Range Wireless Infrared Transmission: The Link Budget Compared to RF," *IEEE Wireless Communications*, vol. 10, no. 2, pp. 8-14. Apr. 2003.

28. A. J. C. Moreira, R. T. Valadas and A. M. de Oliveira Duarte, "Optical Interference Procuced by Artificial Light," *Wireless Networks*, pp. 131-140. 1997.

29. D. C. M. Lee, J. M. Kahn and M. D. Audeh, "Trellis-Coded Pulse Position Modulation for Indoor Wireless Infrared Communications," *IEEE Transactions on Communications*, vol. 45, no. 9, pp. 1080-1087. Sept. 1997.

30. F. R. Mireles and R. A. Scholtz, "Multiple-Access Performance Limits With Time Hopping and Pulse Position Modulation," *Proc. of IEEE Military Communications Conference*, vol. 2, pp. 529–533, 1998.

31. http://www.srisaicom.com/prbg.html, June 2004.

32. J. Hansen, "Analytic Calculation of the Power Delay Profile for Single Room Wireless LAN Environments," *IEEE Global Telecommunications Conference*, vol. 1, pp. 98-102, 2000.

33. H. Hashemi, "The Indoor Radio Propagation Channel," *Proceedings of the IEEE*, vol. 81, pp. 943–967, July 1993.

34. H. Hasmemi, "Impulse Response Modeling of Indoor Radio Propagation Channels," *IEEE Journal on Selected Areas in Communications*, vol. 11, pp. 967–978, Sept. 1993.

35. G. J. Foschini and M. J. Gans, "On Limits of Wireless Communications in a Fading Environment When Using Multiple Antennas," *Wireless Personal Communications*, 1998, pp. 311–335.

36. V. Tarokh, N. Seshadri, and A. R. Calderbank, "Space-Time Codes For High Data Rate Wireless Communication: Performance Criterion and Code Construction," *IEEE Transactions on Information Theory*, vol. 44, pp. 744–765, Mar. 1998.

37. S. M. Alamouti, "Simple Transmit Diversity Technique For Wireless Communications," *IEEE Journal on Selected Areas in Communications* vol. 16, pp. 1451–1458, Oct. 1998.

38. V. Venkatesan, "Performance of a Binary Pulse Position Modulated Ultra-Wideband System With Direct Sequence Spreading For Multiple Access," M.S. thesis, Oregon State University, Department of Electrical Engineering and Computer Science, 2004.

39. H. Liu, "Error Performance of MIMO Systems in Frequency-Selective Rayleigh Fading Channels," *Proc. of IEEE Globecom*, vol. 4, pp. 2104–2108, Dec. 2003.

40. J. G. Proakis, *Digital Communications*. New York, NY: McGraw-Hill, 3rd ed., 1995.